Geochimica et Cosmochimica Acta 343 (2023) 49–63

Contents lists available at ScienceDirect

Geochimica et Cosmochimica Acta

journal homepage: www.elsevier.com/locate/gca

Molecular-level evidence of early lipid transformations throughout oceanic depths

Blaženka Gašparović [a,*], Richard S. Lampitt [b], Nilusha Sudasinghe [c], Tanner Schaub [d]

[a] Laboratory for Marine and Atmospheric Biogeochemistry, Division for Marine and Environmental Research, Ruđer Bošković Institute, POB 180, HR-10002 Zagreb, Croatia
[b] National Oceanography Centre, Southampton, United Kingdom
[c] Bioscience Division, Los Alamos National Laboratory, Los Alamos, NM 87545, United States
[d] Chemical Analysis and Instrumentation Laboratory, College of Agricultural, Consumer and Environmental Sciences, New Mexico State University, Las Cruces, NM 88003, United States

ARTICLE INFO

Article history:
Received 4 March 2022
Accepted 17 December 2022
Available online 21 December 2022
Associate editor: Elizabeth Canuel

Keywords:
Lipidomics
Lipid transformation pathways
NE Atlantic Ocean
Epipelagic
Mesopelagic
Bathypelagic
Abyssal
FT-ICR MS

ABSTRACT

Our understanding of lipid biogeochemistry of the ocean's interior is still in its infancy. Here we focus on early lipid transformation and the formation of lipid degradation products in the NE Atlantic Ocean (49.0°N, 16.5°W). We employed high resolution Fourier transform ion cyclotron resonance mass spectrometry (FT-ICR MS), a method that allows observation and elemental composition assignment of thousands of lipids in a single sample. Using these data, we infer molecular-level changes that occur during lipid transformation in the oceanic water column to shed new light on early lipid transformation processes and the formation of lipid decomposition intermediates, here termed CHO compounds (i.e., lipid-derived species that contain carbon, hydrogen and oxygen in their molecular formula). We considered the distribution of molecular rings and/or double bonds (DBE), H/C and O/C ratios, molecular diversity based on the number of mass spectral signals for monoisotopic species, and carbon number in CHO molecules. Data are elaborated for the four ocean zones, the epipelagic, mesopelagic, bathypelagic and abyssal. The highest molecular diversity characterizes CHO compounds associated with the epipelagic zone, which is explained by numerous and diverse planktonic communities inhabiting the epipelagic and by the effects of both biotic and abiotic processes on lipid transformation. Lipid transformations include crosslinking (condensation), partial degradation or fragmentation, double bond reduction, oxidation, hydrogenation, dehydrogenation and cyclization. Crosslinking likely results in a unimodal distribution of carbon number of CHO compounds, in contrast to cell lipids (referred to as Reported lipids based on the Lipid Maps Database), which have a bimodal distribution of carbon number. CHO compounds that appear to be formed by fragmentation (decrease of the number of C atoms) and ring/double bond reduction were more stable to further transformation and remained longer in the water column, i.e., these compounds were transferred deeper into the water column. Low unsaturation and fast transport to depth promotes CHO compound preservation in the water column. Dehydrogenation leads to increased unsaturation (average DBE up to 21.3), condensation, and cyclization, resulting in high molecular weight compounds with a high degree of unsaturation. Our data demonstrate that lipids with cyclic structures are more refractory than those with acyclic structures. The formation of aromatic structures is not a significant process during early lipid transformation in the oceanic water column.

1. Introduction

The oceans play a vital role in moderating the Earth's climate through carbon and nutrient cycling. This is of great interest as the ocean has a large capacity to absorb atmospheric CO_2 and, hence, mitigate the effect of human emissions of this greenhouse gas. The entire mechanism of carbon removal from the atmosphere by living organisms by the so-called biological pump and connected influential factors is still not well understood. The interplay of biological, chemical and physical processes in the oceans provides an efficient mechanism for the production of new organic carbon as well as for its recycling. Particulate organic matter produced by living organisms changes qualitatively and quantitatively while sinking through the water column (Wakeham and Lee, 1993). With increasing depth, the proportion of uncharacterized organic matter (OM) increases. This OM fraction constitutes >80% of the organic carbon in the deep ocean (Lee et al., 2004).

* Corresponding author.
E-mail address: gaspar@irb.hr (B. Gašparović).

https://doi.org/10.1016/j.gca.2022.12.021
0016-7037/

The OM formation mechanisms, their composition, and information about the unidentified OM are the main interest of geochemists (Wakeham et al., 1997a, 1997b).

Carbohydrates, proteins, and lipids are major biochemical components in the marine environment. Although present in low concentrations, lipids are an integral component of oceanic biomass (Arts et al., 2001). The concentration of total particulate lipids in the open ocean ranges between 3 and 29 μg L^{-1} (Gašparović et al., 2014, 2017), and is higher in coastal ocean areas (3–189 μg L^{-1}; Parrish et al., 1988; Gérin and Goutx, 1994, Galois et al., 1996; Derieux et al., 1998). While total lipid concentration decreases with increasing ocean depth, its relative contribution to particulate organic carbon increases with depth. This suggests a selective accumulation of total lipids with particles sinking with respect to other OM classes (Gašparović et al., 2014, 2017). In addition, there is selective accumulation or degradation of lipid classes; C25-highly branched isoprenoid alkenes are very labile, whereas long-chain vascular plant alkanes can be selectively enriched in sediments (Wakeham et al., 1997a, 2002; Canuel and Martens, 1996). Lipid preservation ability is dependent on the region, i.e., environmental conditions (Wakeham et al., 2002).

Biochemical and geochemical lipid transformation processes occurring in the water column influence lipid composition, abundance, and distribution. The molecular structure of lipids and environmental conditions affect lipid reactivity (Wakeham and Canuel, 2006). Unsaturated OM, including lipids, is generally considered more reactive than saturated OM (Sun and Wakeham, 1994; Canuel and Martens, 1996; Wakeham et al., 1997a, 1997b; Loh et al., 2008). Saturated lipids are more resistant to degradation and are therefore important vectors for carbon sequestration (Gašparović et al., 2016, 2018a).

Some lipids are preserved in the molecular sedimentary record, and may serve as indicators of climatic variation. The chemical resilience of lipids depends on their early diagenetic alterations, which determines their persistence in the water column (Brassell, 1993). There is a possibility of non-selective preservation of labile organic matter, allowing it into sink deeper in the water column. This is made possible by physical protection through encapsulation within refractory organic material and incorporation into resistant coatings and minerals (Hedges et al., 2001; Killops and Frewin, 1994). Lipid alteration and degradation occur via biotic and abiotic processes that often operate in parallel. Biotic transformation (peroxidation, biohydrogenation) (Rontani and Koblízek, 2008) involves the activity of exo- and endo-enzymes on lipids. Abiotic transformation includes photooxidation and autoxidation by free radical-mediated oxidation via hemolytic cleavage of photochemically produced hydroperoxides. Photooxidation may be important within the surface productive layer, while autoxidation and biotransformation may occur throughout the water column (Rontani et al., 2009). Versteegh et al. (2004) proposed an oxidative polymerization of unsaturated fatty acids as a mechanism for the preservation of algal organic matter in sediments. These processes control the degree to which the deep ocean can store lipid originated carbon. Preserved lipids and their transformation products can be incorporated into sediments and preserved for millions of years. A comprehensive review of the selective degradation/preservation of organic matter, including lipids, in marine sediments is given by Zonneveld et al. (2010). Alternatively, lipids are incorporated into the humin-like material (called geopolymer) that continues to undergo condensation and defunctionalization, resulting in kerogen (Killops and Killops, 2013).

Our understanding of lipid transformation in the ocean is still in its early stages. Most work on lipid degradation has been focused on sedimentary organic matter processes, including modeling (e.g., the influence of lipid stability on sedimentary pool (Lipp and Hinrichs, 2009), modeling subseafloor lipid profiles to assess the validity of intact polar lipids as proxies of subseafloor biomass (Xie et al., 2013). Abiotic degradation of chlorophyll phytyl chain, carotenoids, D5-sterols, unsaturated fatty acids, alkenones, and unsaturated alkenes in the marine realm has also been investigated (Rontani and Belt, 2020 and references therein). Additional studies have focused on lipid degradation in the ocean water column (Wakeham et al., 1997a, 1997b, 2002; Sheridan et al., 2002; Goutx et al., 2007; Collins et al., 2018; Hunter et al., 2021). Examining the photooxidation of intact polar lipids in surface waters of the West Antarctic Peninsula, Collins et al. (2018) found that photooxidation occurs on a scale comparable to bacterial production and that significant rates of photooxidation are characteristic only of polyunsaturated fatty acids. Here, we aimed to achieve a novel view of early lipid molecular transformations in samples collected in the NE Atlantic Ocean (the Porcupine Abyssal Plain sustained observatory (PAP-SO)) from the epipelagic down to the abyssal. To do this, we employed high-resolution Fourier transform ion cyclotron resonance mass spectrometry (FT-ICR MS). This technique provides both high mass resolving power and sub-part-*per*-million mass measurement accuracy that allows unambiguous elemental composition assignments directly from the measured mass-to-charge ratios for thousands of observed mass spectral signals (McKenna et al., 2014). This approach enabled elucidation of water column-related molecular-level particulate lipid changes. Lipid elemental compositions for which there was no database match were selected for this analysis. Among these unidentified lipids, the compounds containing carbon, hydrogen, and oxygen in the molecular formula are termed CHO compounds. Previously, we studied other unidentified lipids that contain heteroatoms, nitrogen, phosphorus, and sulfur (Gašparović et al., 2017; 2018a, 2018b). We combined CHO compound data with environmental data, including oxygen content, photosynthetically active radiation (PAR), and bacterial hopanoid biomarkers, to identify possible factors affecting lipid transformation.

2. Methods

2.1. Study site and sample collection

Measurements and sample collection was performed during research cruise 87 of the RRS James Cook (May, 31–June 18, 2013) to the Porcupine Abyssal Plain (PAP) observatory site (49.0 °N, 16.5 °W) (Fig. 1) in the NE Atlantic. This site has been studied since 1992, aiming to comprehend connections between the surface and deep ocean (Hartman et al., 2020). The PAP site is situated between the subtropical and subpolar gyres and is isolated from the complexities of the continental slope and the Mid-Atlantic Ridge. Thus, it can be treated as a representative of the open ocean (Lampitt et al., 2010). Generally, at the site, phytoplankton blooms start in February, develop slowly and last for several months (Rumyantseva et al., 2019). The study area has continued to absorb atmospheric CO_2 in recent years, with the carbon sink increasing over time (Macovei et al., 2020). More details on the PAP station can be found in Hartman et al. (2012).

Water samples were collected by predawn deployment of a 24 × 20 L SeaBird CTD-Niskin rosette sampler. Five to ten liter samples were collected at depths from the surface (2 m) to 4800 m (50 m above bottom) to encompass the epipelagic (0–100 m), mesopelagic (100–1000 m), bathypelagic (1000–4000 m) and abyssopelagic (4000–4800 m) zones. The particles within the water column collected by the Niskin bottles experience a wide range of sinking velocities prior to collection (Iversen and Lampitt, 2020), and will therefore have resided in different parts of the water column for different time. Although Niskin bottles

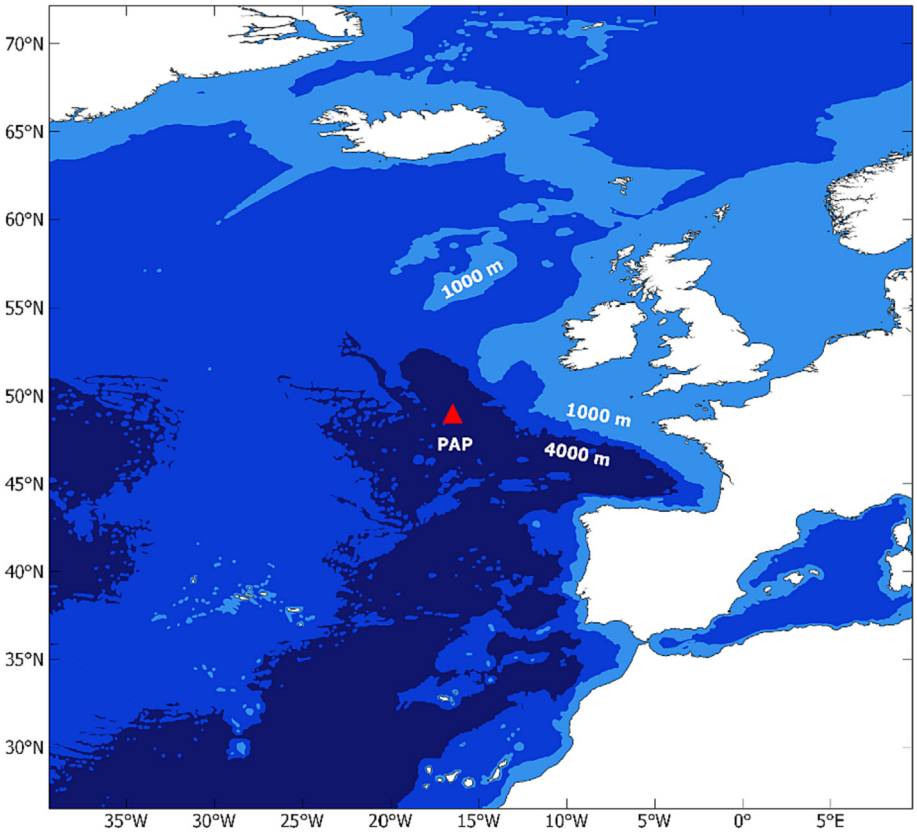

Fig. 1. Map of PAP site in the northern Atlantic Ocean.

primarily collect suspended matter, sinking particles were also collected.

Six of the surface productive layer sampled depths (2–50 m depth) corresponded to 97, 55, 20, 7, 5 and 1% of surface irradiance intensity.

Samples for analysis of particulate lipids were collected by vacuum filtration of the oceanic water on 0.7 μm combusted (450 °C/5h) Whatman GF/F filters, following our long-term particle collection methodology. However, small particles in the colloidal size range can pass through GF/F filters (Taguchi and Laws, 1988).

After sampling, the filters were frozen immediately and stored at −80 °C until extraction. Temperature, salinity, oxygen and PAR measurements were made using Seabird SBE 37-IM recorders (Sea-Bird Electronics Inc., Bellevue, Washington, USA).

2.2. Lipid analysis

Extraction of lipids was performed using a modified one-phase solvent mixture of dichloromethane/methanol/water (1:2:0.8 v:v:v) following the Bligh and Dyer method (Bligh and Dyer, 1959). In brief, lipids from the filters were washed twice with the one-phase solvent mixture, once with the bi-phase solution (dichloromethane/0.73% NaCl solution, 1:1 v/v) and twice with dichloromethane. After each wash, the lipids were separated by filtration through a sinter funnel into a separatory funnel. One microgram of the internal standard reserpine was added to each sample before extraction. Extracts were concentrated to dryness under nitrogen flow and stored at –20 °C until analysis.

Particulate-derived lipid material was analyzed by direct-infusion electrospray ionization Fourier transform ion cyclotron resonance mass spectrometry (ESI FT-ICR MS) in both positive and negative ionization modes, with a hybrid linear ion trap 7T FT-ICR mass spectrometer (LTQ FT, Thermo Fisher, San Jose, CA) equipped with an Advion Triversa NanoMate (Advion Biosystems, Inc.) as previously described (Holguin and Schaub, 2013; Gašparović et al., 2018b). The electrospray solutions for positive ion mode include 1 mM sodium acetate, which facilitates formation of predominantly sodium-adducted ions. For the Triversa electrospray robot, the ionization voltage was −1.2 kV for negative ion mode and +1.7 kV for positive ion mode, with a backing pressure of 0.1 PSI in both cases. The ion transfer capillary temperature was 250 °C and the tube lens voltage was minimized (20 V) to avoid nozzle-skimmer dissociation of the analyte ions. FT-ICR MS data were acquired for ~3 s at a mass resolving power of $m/\Delta m_{50\%}$ = 400,000 at m/z 400. A total of 500 time-domain transients were co-added for each sample prior to fast Fourier transformation and frequency-to-m/z ratio conversion.

Peak lists were generated from each mass spectrum at a peak-picking threshold of S/N (FT-ICR MS signal magnitude for each peak divided by the root mean square magnitude of the noise) > 10. Internal calibration of the mass spectra was performed using homologous alkylation series of reported compounds where elemental compositions differ by integer multiples of CH_2 as is common for natural organic matter (McDonough et al, 2020) and petroleum analyses (Rogers et al., 2005; McKenna et al., 2014). Measured masses for singly charged ions were converted from IUPAC scale (i.e., CH_2 = 14.01565 Da) to the Kendrick mass scale (i.e., CH_2 = 14.0000 Kendrick mass units) as previously described (Kendrick, 1963) and sorted to identify homologous series that are comprised of compound signals with the same heteroatom composition and the same double-bond equivalent value (DBE, the number of molecular rings and/or double bonds to carbon), but different degrees of alkylation. DBE is calculated as follows: DBE = C + 1 − H/2 + N/2. Finally, mass spectral peak magnitude

was normalized to that of the internal standard, reserpine, for each data set, such that mass spectral signals for each compound were normalized to a fixed volume of sampled seawater.

Sub-ppm mass measurement accuracy (defined as <1 ppm RMS mass measurement error for all measured signals) and high mass resolving power combined with Kendrick mass sorting and isotopic fine structure analysis enables robust determination of elemental compositions for individual lipid compounds present in these extracts. No corrections for ionization efficiency/response factors are applied as these values are only available for a negligible proportion of naturally occurring marine lipids. Following elemental composition assignment, we utilized an in-house assembled lipid library derived from Lipid Maps (https://www.lipidmaps.org/, including both the Lipid Maps Structure Database and the in-silico structure database), and matched observed elemental compositions to reported lipids, as previously reported (Holguin and Schaub, 2013; Bartley et al., 2013; Campos et al., 2014; Juergens et al., 2015; Gašparović et al., 2016, 2017, 2018a, 2018b). This database includes original Lipid Maps entries as well as multiple compound types that we have observed in extensive lipidomic characterization of marine microalgae. The additions include compounds from extended Kendrick series for previously-reported compound classes (such as additional and fewer CH_2 acyl moieties) unreported lipid classes specific to marine microalgae (Holguin and Schaub, 2013) and odd carbon number acyl chain combinations for all lipid classes. For the purposes of this effort, elemental compositions for which multiple database isomeric matches are possible, further identification was not attempted. In cases where we discuss specific lipid molecular classes, those compounds represent elemental compositions for which only one database match was made. Furthermore, when discussing specific elemental compositions, the term "compound" is utilized here, with the caveat that multiple isomers can contribute to each observed mass spectral signal. Mass spectral relative abundance is normalized at each depth to the lowest measured peak magnitude across the depth profile.

2.3. Statistical methods

The sample data were tested to determine whether they were drawn from a normally distributed population (Shapiro-Wilk normality test) and whether the data came from populations with equal variances (Two-sample *t*-test for variance) using computer software Origin 7 (Origin Lab). The results indicated that the data are normally distributed with non-equal variance. The sample sizes are non-equal. To test whether there were differences in the population means of CHO compounds and known lipids for DBE, number of C atoms, DBE/C, H/C and O/C (data presented in Figs. 4, 5, 7, and 8 and in Table 1) between the different ocean zones we performed Welch ANOVA followed by post-hoc Tukey-Kramer tests. Statistical analyzes were performed using the software package R and included core packages as well as programs from the packages base, readxl and dplyr. The level of statistical significance was accepted at $p < 0.05$. Linear fits were performed (computer software Origin 7, Origin Lab) to examine the correlations between reported lipids and CHO compounds as well as CHO compounds and unreported compounds that contain heteroatoms (CHONPS compounds).

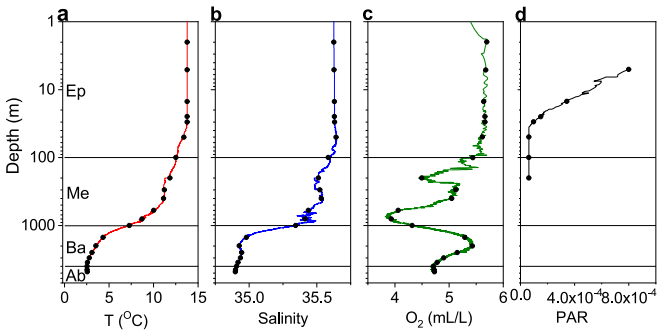

Fig. 2. Depth distribution of temperature (T) (a), salinity (b), oxygen (O_2) (c) and photosynthetic active radiation (d). Symbols represent sampling depths and horizontal lines show the boundaries between ocean zones: the epipelagic (Ep; 0–100 m), mesopelagic (Me; 100–1000 m), bathypelagic (Ba; 1000–4000 m) and abyssopelagic (Ab; 4000–4800 m). Raw data are given in Supplementary Table S1.

3. Results

3.1. Basic oceanographic conditions

In the upper 30 m of the water column, the temperature was 13.78 °C. With increasing depth, the water temperature slowly decreased to 2.55 °C at 4800 m depth (Fig. 2a). Salinity variations generally followed the same trend as temperature variations (Fig. 2b). Surface salinity (35.63) decreased to 34.90 at 4800 m depth. Oxygen concentration (Fig. 2c) varied around 5.65 mL/L in the first 40 m depth. Oxygen depletion varied substantially in the mesopelagic zone. Two minimum oxygen concentrations were observed (4.44. mL/L at 204 m and 3.85 mL/L at 732 m depths). Oxygen concentration increased below 1000 m depth. The concentration of inorganic nutrients increased with depth (Gašparović et al., 2017). Photosynthetically active radiation at 50 m depth was 1% of that of the surface (Fig. 2d).

3.2. Lipid transformation

Thousands of lipid signals were detected using the FT-ICR MS approach in both negative and positive ionization modes. Of the 3,596 monoisotopic lipid compounds detected in the positive ion mode (excluding contributions from ^{13}C and other heavy nuclide-containing species), 2,987 (81.7%) lipid compositions did not match those in the Lipid Maps library (https://www.lipidmaps.org/). In the negative ionization mode, 4,908 monoisotopic lipids were detected, of which 3,654 (74.4%) elemental compositions were not reported in the Lipid Maps database. Raw FT-ICR MS data of both negative and positive ionization modes are given in Supplementary Table S2. Because these unidentified molecular formulas were not found in the database and these compounds were extracted with dichloromethane, an organic solvent (the basic characteristic that defines lipids), these compounds were considered lipid transformation/degradation products.

To interrogate lipid transformation processes, we monitored unidentified lipids that contain carbon, hydrogen, and oxygen in the molecular formula, termed CHO compounds. We identified 1,764 and 1,271 monoisotopic CHO compounds in positive and negative ionization modes, respectively. The data are grouped by the zone(s) in which they were detected and we designate annotation here to facilitate discussion. Zones include: the epipelagic (Ep; 0–100 m; sampled depths: 2, 5, 15, 25, 30 and 50 m), mesopelagic (Me; 100–1000 m; sampled depths: 100, 200, 300, 400, 600 and 800 m), bathypelagic (Ba; 1000–4000 m; sampled depths: 1000, 1500, 2000, 2500, 3000 and 3500 m) and abyssopelagic (Ab; 4000–4800 m; sampled depths: 4000, 4500 and 4800 m). Zero PAR at 100 m depth defined the first depth of the mesopelagic. The increase in O_2 concentration at a depth of 1000 m compared to 800 m defined the beginning of the bathypelagic, while stable oxygen concentrations at 4000, 4500, and 4800 m depth defined the abyssal. CHO compound formulae that were found only in the epipelagic zone are termed CHO_Ep. Similarly, compounds

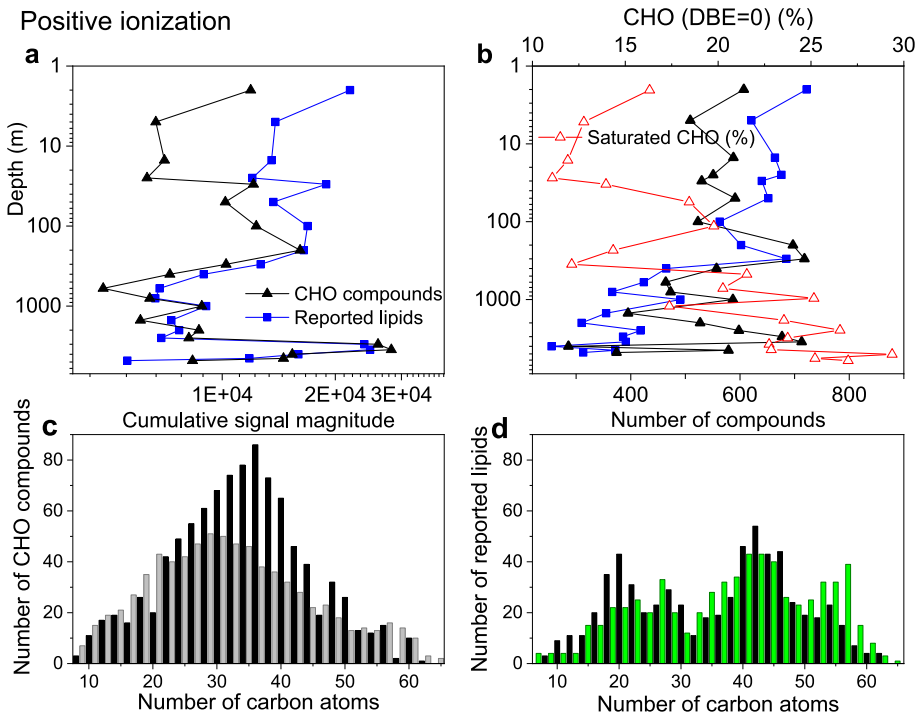

Fig. 3. CHO compounds (triangles) and reported lipids (squares) detected in the positive ion mode. ESI FT-ICR MS cumulative signal magnitudes (a), the total number of mass spectral signals (diversity) and the contribution of the number of mass spectral signals of saturated (DBE = 0) CHO compounds to total CHO compounds (b). The number of CHO compounds (c) and reported database-matched lipids (d) with carbon content in the molecule ranging from 7 to 65. The dark and light columns in (c) and (d) represent even- and odd-carbon number molecules, respectively.

found at depths that range from the epipelagic to the mesopelagic are termed CHO_Ep-Me. Compounds found from the epipelagic, through mesopelagic and to bathyal depths are termed CHO_Ep-Ba. Finally, CHO compounds found from the epipelagic, through the mesopelagic and the bathyal to abyssal depths are termed CHO_Ep-Ab, and these compounds are collectively referred to as CHO compounds connected to the epipelagic. The same holds for CHO compounds related to the mesopelagic, CHO compounds related to the bathypelagic and CHO compounds related to the abyssal. This approach allowed us to describe the early transformation of lipids and their derivatives in the oceanic water column.

Samples were analyzed in both positive- and negative-ion modes to obtain compositional information on as many compounds as possible. Ionization generally reflects compound gas-phase acidity or basicity for negative and positive ion modes, respectively. Among CHO compounds, 418 (24%) and 314 (25%) in the positive and negative ionization modes, respectively, were detected sporadically (in 1–3 samples throughout the water column), and are not considered for further analysis. We compared the characteristics of CHO compound with those of lipids reported in the Lipid Maps database (i.e., phospholipids, glycolipids, triacylglycerols, wax esters, fatty acids…). The observed compounds whose elemental compositions match lipids reported in the Lipid Maps database are termed ReportedLipid_Ep, ReportedLipid_Me, ReportedLipid_Ba, and ReportedLipid_Ab and indicate the layer in which they were detected, i.e., the epipelagic, mesopelagic, bathyal, and abyssal layers, respectively. This approach allowed us to evaluate early lipid transformation processes. We previously found that the cumulative signal magnitude of the FT-ICR MS measurement is proportional to the total lipid content (Gašparović et al., 2018a). Given the different water column behavior and the properties of the CHO compounds detected in the positive and negative ionization modes, we discuss the data for the two ionization modes separately.

3.2.1. Positive ions

The cumulative FT-ICR MS signal magnitude and molecular diversity (the total number of mass spectral signals, i.e., identified formulas) of CHO compounds throughout the ocean depth are compared with those of reported lipids (Fig. 3a and b). Supplementary Fig. S1a and b show these data for the ocean zones. Because ionization efficiency is variable for different lipid classes and functional groups, we do not compare signal magnitudes between compounds, but rather consider sample-to-sample variation of compound signals across the entire depth profile. The cumulative signal magnitude of CHO compounds is proportional to that of reported lipids for the entire water column. Data on CHO compound signal magnitudes are compared with reported lipids (R^2 = 0.77, $p < 0.001$) (Supplementary Fig. S1c) and CHO compounds that also include hetero atoms, N and P (R^2 = 0.77, $p < 0.001$) (Supplementary Fig. S1d) (Gašparović et al. 2017). The cumulative signal magnitude of CHO compounds was lowest in the epipelagic, increased until bathyal, and decreased in the abyssal. The total molecular diversity of CHO compounds was lower than that of reported lipids in the epipelagic and higher in the deeper layers (Fig. 3b). In terms of oceanic zones, the diversity of CHO compounds was highest in the mesopelagic (1,179 molecular formulae) and lowest in the abyssal (689 molecular formulae) (Supplementary Fig. S1b). The proportion of saturated (DBE = 0) CHO compounds in the total CHO compound diversity increased continuously from the epipelagic to the abyssal (Fig. 3b) from 12.5% to 22.2% (Supplementary Fig. 1b).

CHO compounds show a unimodal distribution with maximum abundance for molecules with 30–40 C atoms (Fig. 3c) in contrast to the reported lipids that show a bimodal abundance distribution with respect to molecular carbon content (Fig. 3d). Bimodal distribution by number of carbon atoms is an inherent feature of Reported (cell) lipids. Lipids with a smaller number of C atoms (up to ~ 32 C atoms) include fatty acids, cholesterol and derivatives, prostaglandins, C10-C30 isoprenoids, steroids, vitamin

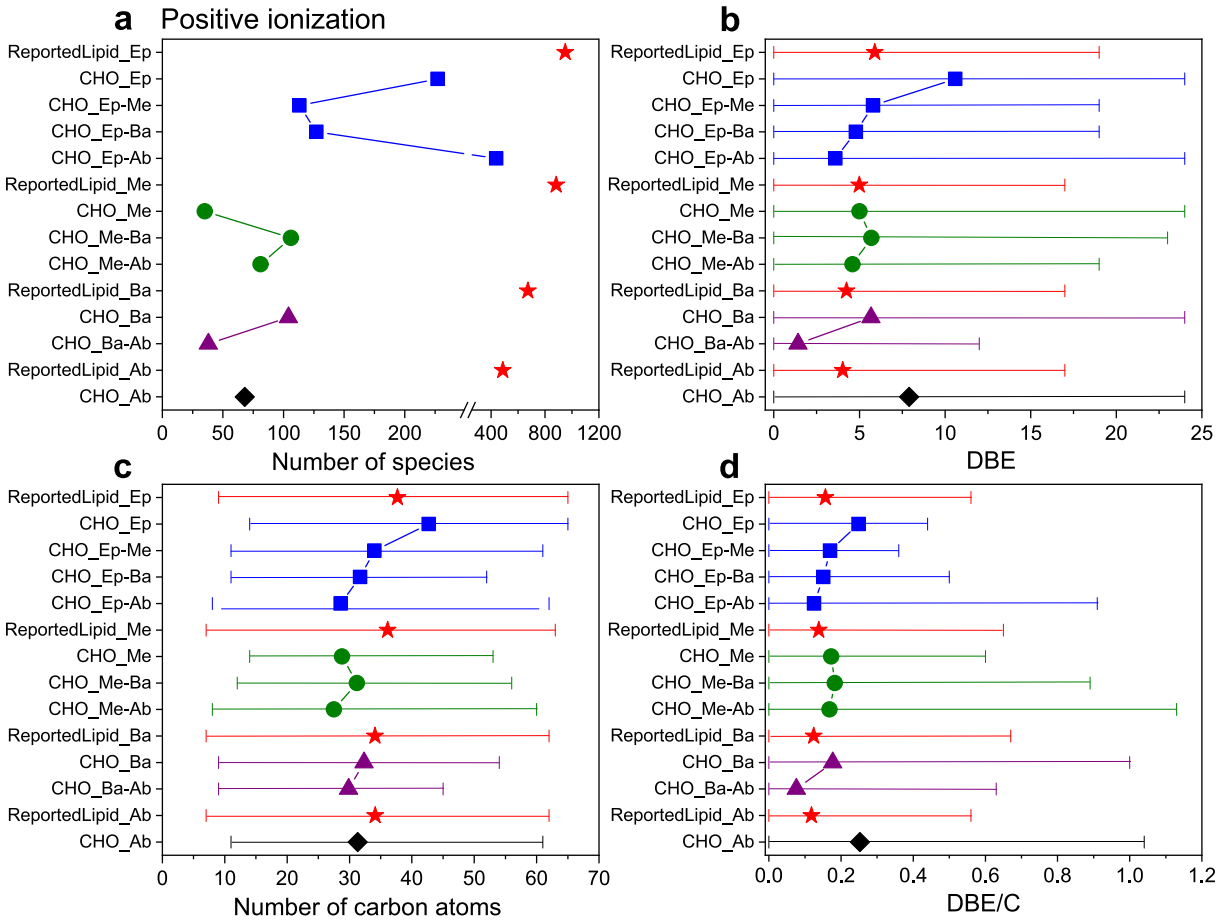

Fig. 4. Positive–ion ESI FT-ICR MS determined reported lipids (stars) and CHO compounds; the average number of monoisotopic peaks (diversity) (a), the average double bond equivalents (DBE) (b), the average number of carbon atoms (c), and the average unsaturation per carbon atom (DBE/C) (d). The "error bars" in b, c, and d indicate data range. Symbols are created as follows: reported lipids – stars, CHO compounds connected to the epipelagic - squares, mesopelagic – circles, bathypelagic – triangles, and abyssal – diamonds. Ep: 0–100 m, Ep-Me: 0–1000 m, Ep-Ba: 0–4000 m, Ep-Ab: 0–4800 m, Me: 100–1000 m, Me-Ba: 100–4000 m, Me-Ab: 100–4800 m, Ba: 1000–4000 m, Ba-Ab: 1000–4800 m and Ab: 4000–4800 m depth.

D... Reported lipids with a larger number of C atoms include triacylglycerols, phospholipids, glycolipids, betaine lipids, wax esters... In the carbon number range 30–40, reported lipids show their lowest abundance. The carbon number-dependent abundance of CHO and reported lipids for the four ocean zones is given in Supplementary Fig. S2. The bimodal distribution of the reported lipids and the unimodal distribution of CHO compounds was preserved in each zone. Unimodal distributions are commonly observed for naturally-occurring organic mixtures including petroleum and dissolved organic matter (Rogers et al., 2005; Kujawinski et al., 2004).

To study the influence of abiotic and biotic processes on the CHO compound production and transformation we correlated the cumulative signal magnitudes and diversity of CHO compounds with oxygen content (oxidation) (Supplementary Fig. S3a and d), with photosynthetically active radiation (PAR, photochemical processing) (Supplementary Fig. S3b and e), and with the cumulative signal magnitude for hopanoids as bacterial biomarkers (biotic processing) (Supplementary Fig. S3c and f). Hopanoids are produced by many different types of bacteria that play a role in the cell membrane (Sáenz et al., 2015) and are used here as a rough measure of bacterial abundance. It should be noted, however, that hopanoids may be underestimated because free-floating bacteria and archaea can pass through GF/F filters during filtration (Taguchi and Laws, 1988). The depth distribution of cumulative signal magnitude and molecular weight (486.44–562.46 Da) of hopanoid biomarkers, determined in the same samples as CHO compounds by FT-ICR MS in positive mode, is shown in Supplementary Fig. S4. The only statistically significant correlation was the negative relationship between CHO compound cumulative signal magnitude and PAR.

The molecular diversity and properties of CHO compounds (DBE, carbon number (C), and unsaturation per carbon atom (DBE/C)) detected in one or more ocean zones are shown in Fig. 4 and are compared with the reported lipids detected in the four ocean zones. The highest molecular diversities were observed for the CHO compounds associated with the epipelagic layer, being CHO_Ep, CHO_Ep-Me, CHO_Ep-Ba, and CHO_Ep-Ab (Fig. 4a). The average DBE value of the CHO compounds produced and degraded within one layer, CHO_Ep, CHO_Ba, and CHO_Ab, were higher compared to reported lipids (Fig. 4b, post-hoc Tukey-Kramer test $p < 0.05$, Supplementary Table S3a). The average degree of molecular unsaturation decreases with final observed depth for particular CHO compounds, significant for CHO_Ep *versus* CHO_Ep-Ab and CHO_Ba *versus* CHO_Ba-Ab (post-hoc Tukey-Kramer test $p < 0.05$, Supplementary Table S3a). The average carbon content was relatively high for CHO compounds throughout the water column, ranging from 27.5 to 42.7 C atoms. The carbon number was lower for CHO compounds associated with the epipelagic that reached deeper in the water column (e.g., CHO_Ep-Ab) (Fig. 4c, post-hoc

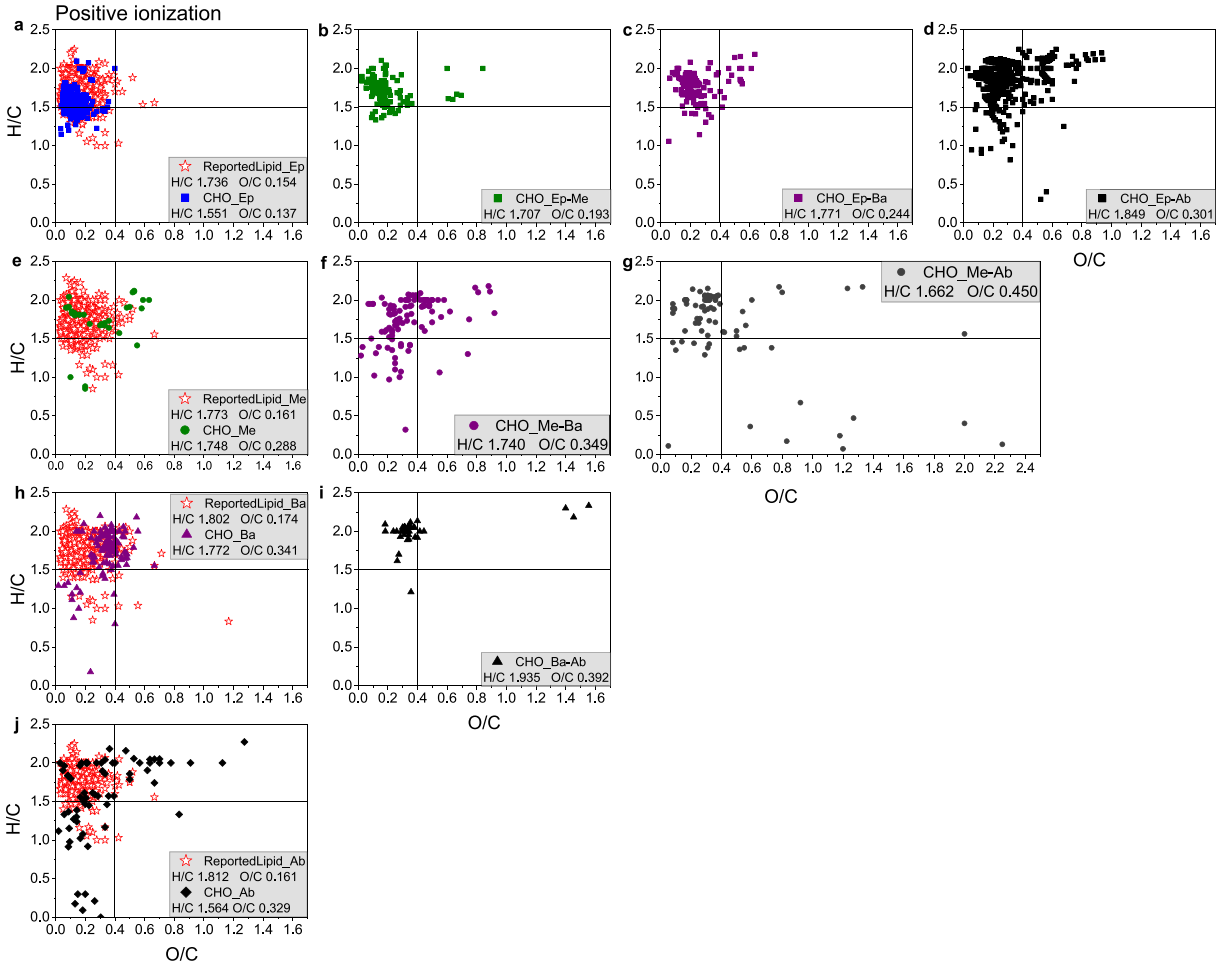

Fig. 5. The van Krevelen diagrams for the CHO compounds detected in the positive-ion ESI FT-ICR MS. symbols are created as follows: Reported lipids – open stars, CHO compounds connected to the epipelagic - squares, mesopelagic – circles, bathypelagic – triangles, and abyssal – diamonds. for on-line readers: CHO compounds that were found only at the epipelagic are shown in blue, those formed at the mesopelagic or reached from the epipelagic to the mesopelagic are shown in green, those that were formed at the bathyal or reached from the epipelagic and mesopelagic to the bathyal are shown in violet, and those that were formed at the abyssal or reached from the epipelagic, mesopelagic and bathypelagic to the abyssal are shown in black. The average H/C and O/C ratios of the reported and CHO compounds are shown in each diagram. Ep: 0–100 m, Ep-Me: 0–1000 m, Ep-Ba: 0–4000 m, Ep-Ab: 0–4800 m, Me: 100–1000 m, Me-Ba: 100–4000 m, Me-Ab: 100–4800 m, Ba: 1000–4000 m, Ba-Ab: 1000–4800 m and Ab: 4000–4800 m depth. The abbreviations are explained in the Results section.

Tukey-Kramer test $p < 0.05$, Supplementary Table S3b). With increasing depth reached by CHO compounds, the average unsaturation per carbon atom and DBE/C of the compounds associated with the epipelagic and bathyal decreased (Fig. 4d, post-hoc Tukey-Kramer test $p < 0.05$, Supplementary Table S3c). The average molecular weight (M_w) of CHO compounds ranged between 529.17 and 691.31 Da (Supplementary Fig. S5). An exception is that of CHO compounds associated with the bathyal, whose molecular weights were much higher than those of reported lipids detected in the bathyal, due to a larger number of oxygen atoms in the CHO compound molecules.

A further illustration of the molecular changes in the distributions of CHO compound is shown in the van Krevelen diagrams (Fig. 5). The horizontal line at H/C = 1.5 represents a molecular lability boundary, as introduced by D'Andrilli et al. (2015), which divides data in the van Krevelen diagrams into more labile ($H/C \geq 1.5$) and more recalcitrant compounds ($H/C < 1.5$). We introduced a vertical line at O/C = 0.4 because the majority, 98%, of the reported lipids have an $O/C \leq 0.4$. The line divides the CHO compounds into those with $O/C \leq 0.4$ and those with $O/C > 0.4$, which are CHO compounds formed by oxidation in the ocean. Most of the reported lipids are within $H/C \geq 1.5$ and $O/C \leq 0.4$, as are many CHO compounds.

A general observation for CHO compounds is that there were three major transformational changes. The first is a transformation to a more oxidized state (Fig. S6b), i.e., compounds for which O/C ratio was >0.4 (Fig. 5). The average O/C ratio increased with the terminal depth reached by CHO compounds. For example, the average O/C ratio of ReportedLipid_Ep is 0.154, and that ratio increases for CHO compounds in the order of CHO_Ep (O/C = 0.137) < CHO_Ep-Me (O/C = 0.193) < CHO_Ep-Ba (O/C = 0.244) < CHO_Ep-Ab (O/C = 0.301) (post-hoc Tukey-Kramer test $p < 0.05$, Supplementary Table S4b).

The second process is hydrogenation, i.e., H/C ratio of the CHO compounds was mainly higher compared to the reported lipids (Fig. S6a and S7, Supplementary Table S4a). The highest average H/C ratios are observed for CHO_Ep-Ab (H/C = 1.849) and CHO_Ba-Ab (H/C = 1.935), which had the highest contribution of saturated compounds, 23 and 38%, respectively. CHO_Me_Ab were also characterized with a high contribution of saturated CHO compounds (21%). As expected, the higher the H/C ratio the lower the DBE for both the reported lipids and the CHO compounds (Fig. S7b).

The third process is the formation of less-hydrogenated substances with H/C < 1.5. These more recalcitrant lipid derivatives (D'Andrilli et al., 2015) were detected mainly in the abyssal zone and in multiple zones including abyssal (Fig. 5d, g, I, and j). Very

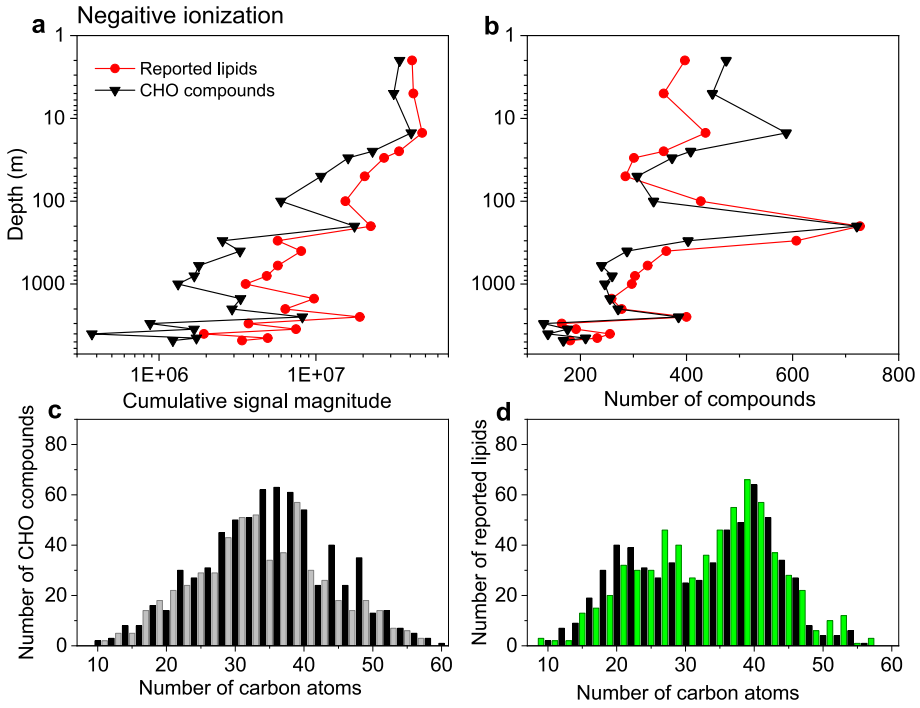

Fig. 6. CHO compounds (triangles) and reported lipids (cyrcles) detected in the negative ion mode. ESI FT-ICR MS cumulative signal magnitudes (a), the total number of mass spectral signals (diversity) (b). The number of CHO compounds (c) and reported database-matched lipids (d) with carbon content in the molecule ranging from 8 to 60. The dark and light columns in (c) and (d) represent even- and odd-carbon number molecules, respectively.

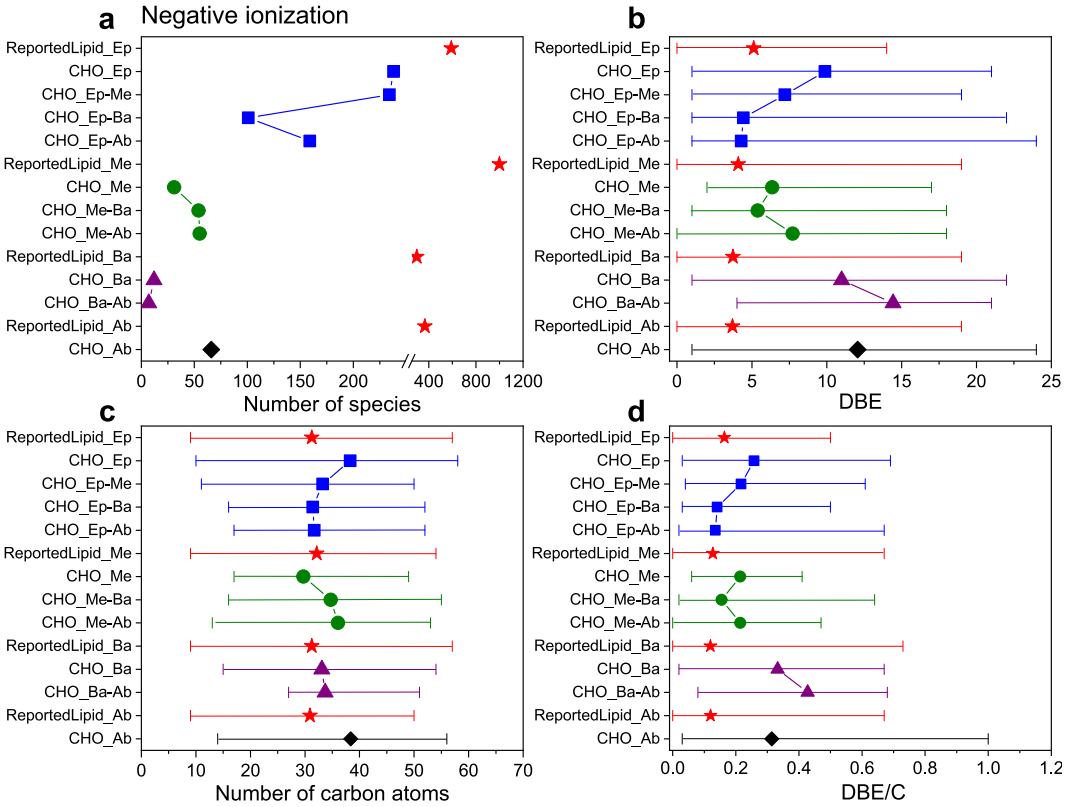

Fig. 7. Negative-ion FT-ICR MS determined reported lipids (stars) and CHO compounds; the average number of monoisotopic peaks (diversity) (a), the average double bond equivalents (DBE) (b), the average number of carbon atoms (c), and the average unsaturation per carbon atom (DBE/C) (d). The "error bars" in b, c, and d indicate data range. Symbols are created as follows: reported lipids – open stars, CHO compounds connected to the epipelagic - squares, mesopelagic – circles, bathypelagic – triangles, and abyssal – diamonds. Ep: 0–100 m, Ep-Me: 0–1000 m, Ep-Ba: 0–4000 m, Ep-Ab: 0–4800 m, Me: 100–1000 m, Me-Ba: 100–4000 m, Me-Ab: 100–4800 m, Ba: 1000–4000 m, Ba-Ab: 1000–4800 m and Ab: 4000–4800 m depth.

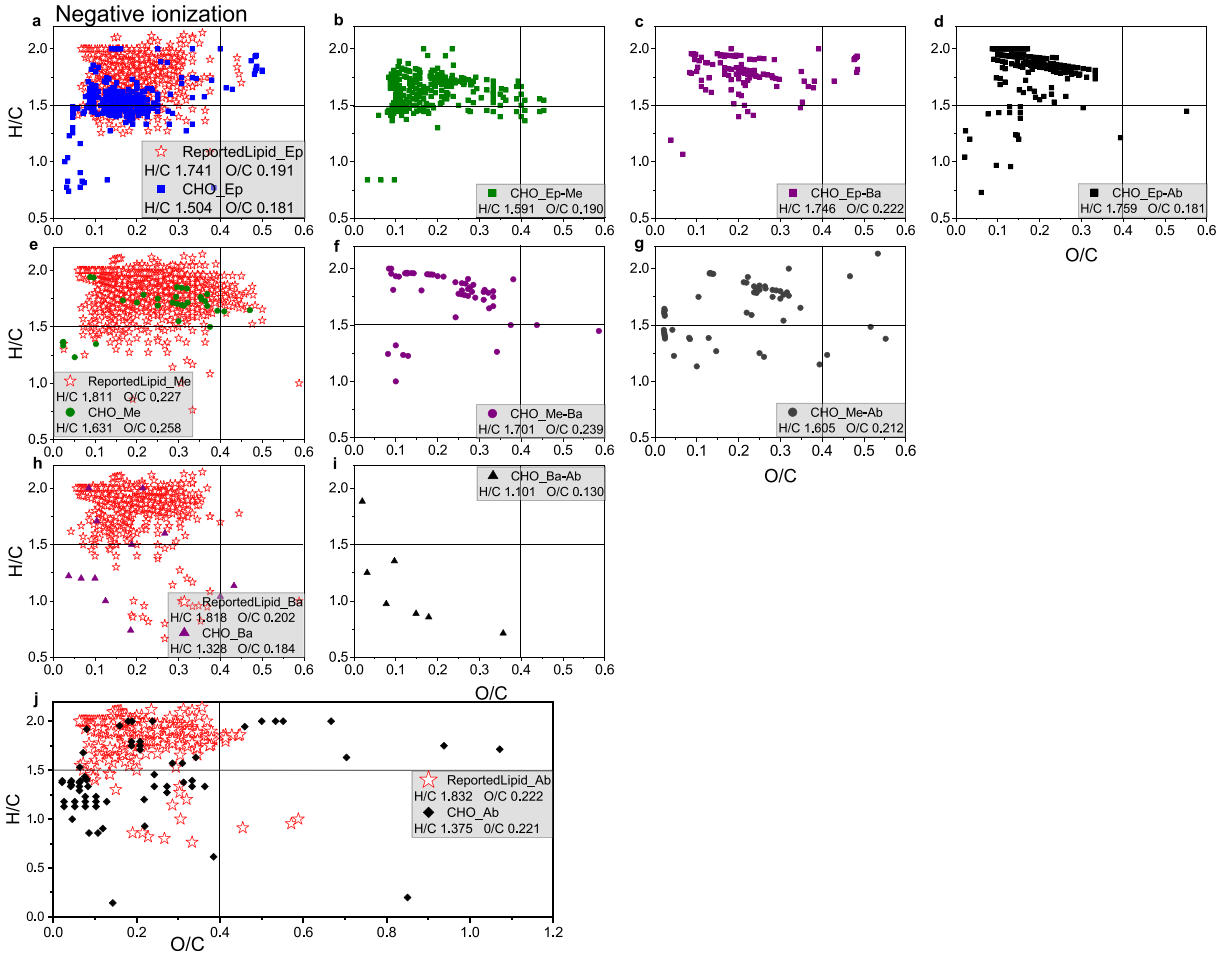

Fig. 8. The van Krevelen diagrams for the CHO compounds detected in the negative-ion ESI FT-ICR MS. The abbreviations are explained in the Results section. Symbols are created as follows: Reported lipids – open stars, CHO compounds observed in the epipelagic - squares, mesopelagic – circles, bathypelagic – triangles, and abyssal – diamonds. For on-line readers: CHO compounds that were found only at the epipelagic are shown in blue, those formed at the mesopelagic or reached from the epipelagic to the mesopelagic are shown in green, those that were formed at the bathyal or reached from the epipelagic and mesopelagic to the bathyal are shown in violet, and those that were formed at the abyssal or reached from the epipelagic, mesopelagic and bathypelagic to the abyssal are shown in black. The average H/C and O/C ratios of the reported and CHO compounds are shown in each diagram. Ep: 0–100 m, Ep-Me: 0–1000 m, Ep-Ba: 0–4000 m, Ep-Ab: 0–4800 m, Me: 100–1000 m, Me-Ba: 100–4000 m, Me-Ab: 100–4800 m, Ba: 1000–4000 m, Ba-Ab: 1000–4800 m and Ab: 4000–4800 m depth. The abbreviations are explained in the Results section.

few of these recalcitrant lipids were aromatic structures (Koch and Dittmar, 2006).

The average DBE, carbon number, and unsaturation per carbon atom (DBE/C) of more labile (H/C $\geq$ 1.5 and O/C $\leq$ 0.4), more oxidized (O/C > 0.4), and more recalcitrant (H/C < 1.5) CHO compounds and reported lipids are listed in Table 1a. The average molecular DBE decreased mainly with depth for both more labile CHO compounds and reported lipids (post-hoc Tukey-Kramer test $p < 0.05$, Supplementary Table S5a). Carbon number and DBE/C decreased with depth, particularly for those CHO compounds associated with the epipelagic (post-hoc Tukey-Kramer test $p < 0.05$, Supplementary Table S5b and c). The average carbon number and DBE/C were mainly higher for the more labile CHO compounds produced and recycled within the epipelagic zone with respect to reported lipids (post-hoc Tukey-Kramer test $p < 0.05$, Supplementary Table S5b and c).

The more oxidized CHO compounds (O/C > 0.4) have the lowest degree of unsaturation and the lowest carbon number compared to the more labile and more recalcitrant CHO compounds, while DBE/C did not differ noticeably between them. With respect to reported lipids characterized by H/C $\geq$ 1.5 and O/C > 0.4 (mainly dicarboxylic acids, oxo acids, hydroxyl acids and some monoacyl phospho- and glycolipids), the more oxidized CHO compounds were more rich in carbon, had variable average DBE and lower DBE/C ratio, albeit not statistically significant (Supplementary Table S6).

The more recalcitrant CHO compounds (H/C < 1.5) had the highest unsaturation and consequently the highest DBE/C. The majority of the recalcitrant CHO compounds were not aromatic, as only 27 of 215 molecular formulas met the criteria for aromaticity (Koch and Dittmar, 2006). The DBE/C increased for the recalcitrant CHO compounds associated with the epipelagic that reached the abyssal (post-hoc Tukey-Kramer test $p < 0.05$, Supplementary Table S7c). The latter have more C atoms in the molecules compared to the reported lipids that satisfy criteria H/C < 1.5 (mainly lipids that contain cyclic and aromatic structures with or without aliphatic chain(s), e.g. flavones, isoprenoids, steroids, vitamin D3, prostaglandins and their derivatives) (post-hoc Tukey-Kramer test $p < 0.05$, Supplementary Table S7b).

3.2.2. Negative ions

The cumulative signal magnitude of CHO compounds detected as negative ions was highest in the epipelagic, decreased by 98% in the abyssal, and followed the depth-related trend of reported lipids (Fig. 6a). Supplementary Fig. S8a shows these data for the ocean zones. The cumulative signal magnitude of CHO compounds

Table 1
The average double bond equivalents (DBE), the average carbon number (C), and double bonds per carbon atom (DBE/C) of labile (H/C ≥ 1.5, O/C ≤ 0.4), more oxidized (O/C > 0.4) and more recalcitrant (H/C < 1.5) CHO and reported lipids. Data are sorted according to the van Krevelen diagrams (Fig. 5). Data are given for the positive (a) and negative (b) ionization. Bolded are data to make distinction between different zones. The abbreviations are explained in the Results section.

Double bond equivalents (DBE), carbon number (C), and double bond equivalents per carbon atom (DBE/C)											
(a) Positive ionization											
		CHO compounds									
		CHO_ Ep	CHO_ Ep-Me	CHO_ Ep-Ba	CHO_ Ep-Ab	**CHO_ Me**	**CHO_ Me-Ba**	**CHO_ Me-Ab**	CHO_ Ba	CHO_ Ba-Ab	**CHO_ Ab**
More labile	DBE	9.1	5.4	4.5	3.0	**4.0**	**3.9**	**2.2**	4.2	1.3	**4.0**
H/C ≥ 1.5	C	43.3	35.6	33.3	30.3	**32.0**	**33.3**	**31.3**	34.4	32.5	**36.1**
O/C ≤ 0.4	DBE/C	0.21	0.15	0.14	0.10	**0.13**	**0.12**	**0.07**	0.12	0.04	**0.11**
More oxidized	DBE	–	4.0	2.0	2.0	**2.2**	**2.4**	**7.4**	3.7	0.5	**1.5**
O/C > 0.4	C		21.8	19.7	19.1	**19.5**	**23.0**	**18.1**	23.9	13.8	**19.7**
	DBE/C		0.18	0.10	0.10	**0.11**	**0.10**	**0.41**	0.15	0.04	**0.08**
More recalcitrant	DBE	13.1	9.2	12.2	14.6	**21.3**	**16.1**	**11.8**	16.0	14.8	**17.3**
H/C < 1.5	C	41.9	27.6	33.1	35.8	**36.3**	**39.3**	**30.8**	38.7	31.3	**33.9**
	DBE/C	0.31	0.33	0.44	0.41	**0.59**	**0.41**	**0.38**	0.41	0.47	**0.51**
		Reported lipids									
		ReportedLipid _Ep				**ReportedLipid _Me**			ReportedLipid _Ba		**ReportedLipid_Ab**
H/C ≥ 1.5	DBE	5.6				**4.8**			4.1		**3.8**
O/C ≤ 0.4	C	38.6				**37.0**			35.2		**35.1**
	DBE/C	0.15				**0.14**			0.12		**0.12**
	DBE	3.4				**2.3**			3.4		**2.3**
O/C > 0.4	C	16.6				**13.3**			16.4		**13.4**
	DBE/C	0.27				**0.23**			0.23		**0.23**
H/C < 1.5	DBE	9.6				**9.2**			8.5		**8.6**
	C	29.0				**26.0**			20.7		**21.3**
	DBE/C	0.34				**0.37**			0.41		**0.41**
(b) Negative ionization											
		CHO compounds									
		CHO_ Ep	CHO_ Ep-Me	CHO_ Ep-Ba	CHO_ Ep-Ab	**CHO_ Me**	**CHO_ Me-Ba**	**CHO_ Me-Ab**	CHO_ Ba	CHO_ Ba-Ab	**CHO_ Ab**
More labile H/C ≥ 1.5	DBE	8.2	6.3	4.0	3.1	**4.6**	**3.5**	**4.7**	4.6	4.0	**4.8**
	C	38.8	33.1	31.5	31.3	**27.2**	**34.8**	**34.7**	34.0	*51**	**37.8**
	DBE/C	0.21	0.20	0.13	0.10	**0.17**	**0.11**	**0.13**	0.15	0.08	**0.12**
More recalcitrant	DBE	12.7	11.1	11.5	13.4	**15.4**	**14.8**	**13.6**	15.6	16.2	**16.0**
H/C < 1.5	C	37.4	33.7	30.0	34.5	**43.0**	**34.6**	**38.4**	32.4	30.8	**38.7**
	DBE/C	0.35	0.34	0.37	0.40	**0.36**	**0.43**	**0.35**	0.49	0.53	**0.44**
		Reported lipids									
		ReportedLipid _Ep				**ReportedLipid _Me**			ReportedLipid _Ba		**ReportedLipid_Ab**
H/C ≥ 1.5	DBE	4.7				**3.8**			3.3		**3.3**
	C	32.1				**33.0**			31.9		**31.4**
	DBE/C	0.15				**0.12**			0.11		**0.11**
H/C < 1.5	DBE	8.5				**8.7**			9.9		**10.4**
	C	25.4				**23.9**			21.0		**22.6**
	DBE/C	0.34				**0.37**			0.48		**0.47**

*Only one compound detected.

was proportional to those of reported lipids for the entire water column and also to the cumulative signal magnitudes of most lipid classes like phospholipids, sulphoquinovosyldiacylglycerols, cholesterols, triacylglycerols (Gašparović et al., 2017, 2018a, 2018b). The CHO compound signal magnitudes are compared to reported lipids (R^2 = 0.74, p < 0.001) (Supplementary Fig. S8c) and also CHO compounds contain heteroatoms N, P, and S (R^2 = 0.82, p < 0.001) (Supplementary Fig. S8d) (Gašparović et al., 2017, 2018a, 2018b). The depth-dependent diversity trend of CHO compounds followed that of reported lipids. Only in the epipelagic, CHO compound diversity (738 formulae) was higher than that of reported lipids (590 formulae) (Fig. 6b, Supplementary Fig. S8b). No saturated (DBE = 0) CHO compounds were detected in the epipelagic zone, and only 1 to 5 species were detected in the deeper zones.

The distribution of molecular abundance of CHO compounds (Fig. 6c, Supplementary Fig. S8) and reported lipids (Fig. 6d, Supplementary Fig. S8b) with molecular carbon content between 8 and 60 had the same unimodal and bimodal distributions, respectively, as observed for the compounds detected in the positive ion mode. The carbon number-dependent abundance of CHO and reported lipids for the four ocean zones can be found in Supplementary Fig. S9. The bimodal distribution of the reported lipids and the unimodal distribution of CHO compounds were preserved in each zone.

The relationships between oxygen concentration (oxidation), PAR (photooxidation), and abundance of bacteria (a rough measure estimated based on hopanoid markers) (Supplementary Fig. S10) with cumulative signal magnitude and diversity of CHO compounds are mainly statistically significant (Fig. S11). These observations suggest that these parameters influence the production of CHO

compounds. The depth distribution of cumulative signal magnitude and molecular weight (526.44–560.45 Da) of hopanoid biomarkers, determined in the same samples as CHO compounds by FT-ICR MS in negative mode, is shown in Supplementary Fig. S10.

As with positive ion, negative ion CHO compounds associated with the epipelagic zone showed much greater molecular diversity than those formed in the mesopelagic and deeper (Fig. 7a). The average degree of unsaturation was highest for CHO compounds produced in the bathyal and abyssal zones. The unsaturation of CHO compounds associated with the epipelagic was lower for those found deeper in the water column (post-hoc Tukey-Kramer test $p < 0.05$, Supplementary Table S8a). The average unsaturation was mainly higher for CHO compounds (average DBE 4.3–14.4) than that of reported lipids (average DBE 3.7–5.1) (Fig. 7b, post-hoc Tukey-Kramer test $p < 0.05$, Supplementary Table S8a).

The average carbon number of the CHO compounds observed in the negative ion mode varied between 28.7 and 38.4C atoms, whereas the average C number for the reported lipids ranged between 30.9 and 32.1 C atoms (Fig. 7c). The average carbon number of CHO compounds produced and degraded within the same layer, CHO_Ep and CHO_Ab, were higher compared to the reported lipids (post-hoc Tukey-Kramer test $p < 0.05$, Supplementary Table S8b). CHO compounds connected to the epipelagic exhibited a concomitant decrease in carbon number in deeper layers (post-hoc Tukey-Kramer test $p < 0.05$, Supplementary Table S8b). The CHO compound molecular weight (Supplementary Fig. S12) ranged from 506.15 to 626.78 Da, following the trend observed for the average carbon number. As observed for positive ions, CHO_Ba and CHO_Ba-Ab deviated from that trend. The unsaturation per carbon followed the trend of DBE (Fig. 7d, post-hoc Tukey-Kramer test $p < 0.05$, Supplementary Table S8c) and ranged between 0.14 and 0.43.

The van Krevelen diagrams for CHO compounds detected in the negative ionization mode (Fig. 8) show that a negligible number of CHO compound formulae had O/C > 0.4 (1–8 compounds). The O/C data of the CHO compounds in the water column (Fig. S13b) had a lower O/C compared to reported lipids. Therefore, we do not discuss highly oxidized CHO compounds detected in the negative ion mode. We observed an average lower H/C ratio for the CHO compounds formed and transported to greater depths, albeit significant for CHO compounds associated with the epipelagic (Figs. 8, S13 and S14, post-hoc Tukey-Kramer test $p < 0.05$, Supplementary Table S9a). The average H/C ratios are 1.76, 1.61, 1.10 and 1.38 for the CHO_ Ep-Ab, CHO_Me-Ab, CHO_Ba-Ab, and CHO_Ab, respectively. The H/C ratios of the reported lipids increased with depth, especially compared to the reported lipids detected in the epipelagic (Fig. 8a, e, h and j, post-hoc Tukey-Kramer test $p < 0.05$, Supplementary Table S9a), possibly due to the depth-related decrease in unsaturation. The average H/C ratios for the reported lipids were 1.74, 1.83, 1.82, and 1.83 in the epipelagic, mesopelagic, bathypelagic and abyssal, respectively. As observed for the CHO compounds detected in the positive ion mode, only a few CHO compound formulae met the criteria for aromaticity (Koch and Dittmar, 2006).

The average DBE, carbon number, and unsaturation per carbon atom (DBE/C) of the CHO compounds detected in the negative ionization mode are listed in Table 1b. Data are presented for more labile ($H/C \geq 1.5$) and more recalcitrant ($H/C < 1.5$) CHO compounds, and for the reported lipids. The reported lipids characterized by $H/C < 1.5$ were mostly cyclic structures such as flavonoids, isoprenoids, steroids, cholesterol and derivatives, and vitamin D and derivatives. The more recalcitrant CHO compounds were characterized by higher DBE in compared to the reported lipids (post-hoc Tukey-Kramer test $p < 0.05$, Supplementary Table S10a).

CHO compounds were often richer in C atoms relative to reported lipids, both those with $H/C \geq 1.5$ and $H/C < 1.5$ (post-hoc Tukey-Kramer tests, Supplementary Table S10b and S11b). The unsaturation per carbon (DBE/C) was mainly higher for the more labile CHO compounds than that of the reported lipids, especially those associated with the epipelagic and mesopelagic (post-hoc Tukey-Kramer test $p < 0.05$, Supplementary Table S11c).

4. Discussion

The pathways and mechanisms of lipid transformation and degradation in the ocean remain mainly unknown. The earliest degradation step of acylglycerols (triacylglycerols, phospholipids, glycolipids, betaine lipids) is the fatty acid cleavage from the glycerol backbone (e.g. Goutx et al., 2003). Rontani and Belt (2020) described the initial transformation of sterols, fatty acids and alkenones. The next steps of lipid transformation are still unexplored, largely because there are no analytical techniques and standards to enable such studies. Our studies of novel lipids (unreported, i.e., not included in the database) containing nitrogen, sulfur, and phosphorus were described previously (Gašparović et al., 2017, 2018a; 2018b), but with a different approach than applied here.

One advantage of the FT-ICR MS technique is the simultaneous determination of tens of thousands of elemental compositions from isomeric species present in complex samples; a capability that facilitates the interrogation of early lipid transformation processes and the formation of lipid decomposition intermediates. The average number of carbon atoms in the observed CHO compounds is close to that of the reported lipids, suggesting that CHO compounds represent early lipid transformation products. We considered molecular diversity as indicated by the number of observed monoisotopic compounds, molecular ring and/or double bond conten (DBE), H/C and O/C ratios, the number of carbon atoms of CHO compound molecules, and signal magnitude as a rough, semi-quantitative measure of abundance indicating the trend of lipid content changes across ocean zones. CHO compound data are compared to reported lipid bulk properties.

4.1. CHO compounds detected at the two ionization modes are mainly different compounds

We observed a difference in the depth-related behavior and molecular characteristics of CHO compounds detected as positive ions compared to those detected as negative ions. In contrast to the CHO compounds identified in the positive ionization mode, the cumulative signal of CHO compounds detected in the negative ionization mode decreased much more until the abyssal zone suggesting that they are more labile (Fig. 6a vs Fig. 3a), less sensitive to oxidation, or oxidation products are very susceptible to transformation/degradation (Fig. 8 vs Fig. 5), their cumulative signal magnitude and diversity are mainly lower with respect to the reported lipids (Fig. 6a vs Fig. 3a). This suggests that largely different CHO compounds are detected in these two modes. Therefore, we have described these lipids separately, however, similar transformation pathways are also observed.

4.2. CHO compound depth distribution

The abundance of CHO compounds, detected with both ionization modes, decreased from the surface layer to the deeper layers, following reported lipid abundance changes across ocean water column (c.f. Fig. 3a and Fig. 6a). This is particularly evident for those measured as negative ions, which appear to be subject to strong biotic (bacteria) and abiotic (irradiation) degradation, with subsequent substantial abundance decrease (98%) to abyssal depths (c.f. Fig. 6 and Fig. S10). Their depth-related loss could be due to transformation of lipids into assimilable components, loss

to the dissolved fraction, decomposition to CO_2, incorporation into bacterial biomass, and into recalcitrant substances. Lipids prove to be important structural components of marine recalcitrant humic substances (Stuermer and Harvey, 1978).

CHO compounds that were detected as positive ions appear to be less susceptible to degradation (c.f. Fig. 3 and Fig. S3). Consequently, compared to CHO compounds observed as negative ions, their molecular diversity is greater, they are more stable, are transferred deeper into the water column, and their quantity decreased only about 29% between the epipelagic and abyssal, and 50% between the mesopelagic and abyssal. The observed increase in cumulative signal magnitude of CHO compounds and reported lipids in the bathypelagic (Fig. 3a) is accompanied by the decrease in temperature and salinity and increase in the dissolved oxygen (Fig. 2a–c). The observed oceanographic changes could be explained by the horizontal intrusion of Labrador Sea water (van Aken, 2000a, 2000b), which is characterized by low salinity (van Aken, 2000b) and high oxygen content (McGrathet al., 2012). It is possible that water from the Labrador Sea contributed an excess of CHO compounds and reported lipids to the bathyal zone. We assume that CHO compounds from the positive ionization, which were extracted from the particles, were efficiently transported to depth by diatom (silicate frustules) and coccolitophoride (calcite coccoliths) remains (Martin et al., 2011; O'Brien et al., 2013). Indeed, pigment analysis of the same samples revealed that nanophytoplankton prymnesiophytes and microphytoplankton diatoms dominated surface samples (Gašparović et al., 2018b). We cannot exclude the possibility that CHO-compounds in the deep ocean originate in part from bacteria and archaea whose lipids have not yet been characterized. A substantial contribution of the saturated CHO compounds is most likely also responsible for the higher stability in the water column of the compounds detected in the positive compared to the negative ionization mode.

The epipelagic is characterized by a great molecular diversity (Fig. 4a and Fig. 7a). Much of the epipelagic CHO compounds may have sunk to greater depths (Fig. 4a and Fig. 7a) and contributed to high molecular diversity in the mesopelagic (Fig. 3b and Fig. 6b).

CHO compounds with lower unsaturation mainly survived transport to greater depths (Fig. 4b and Fig. 7b). For example, the average DBE of CHO_Ep-Ab are 3.6 and 4.3 for positive and negative ionization, respectively, whereas the average DBE of CHO_Ep are 10.6 and 9.9 for positive and negative ionization, respectively. This indicates that CHO compounds with lower unsaturation are transported deeper in the water column from the layer where they were first detected, suggesting that they are more resistant to degradation and that lower unsaturation improves lipid lifetime in the water column.

4.3. The epipelagic is a layer of intense CHO compound formation

CHO compounds associated with the epipelagic zone (detected in both ionization modes) had the highest molecular diversity (Fig. 4a and Fig. 7a). This is due to the presence of numerous and diverse planktonic communities and the influence of various processes (biotic and abiotic), often occurring in parallel, leading to the transformation and degradation of lipids. The much greater molecular diversity of the CHO compounds compared to the CHO compounds that also contain nitrogen, sulfur, and/or phosphorus (Gašparović et al., 2017, 2018a, 2018b) can be understood from the much greater diversity of the reported lipids that contain C, H, and O compared to the reported lipids that also contain N, S, and/or P in the molecular formula. It can be assumed that the removal of the functional group(s) containing N or P is the first step of lipid transformation. However, this could not be proven because the signal magnitudes of CHO compounds and the compounds containing heteroatoms (CHONP and CHONPS) are significantly positively correlated for the whole water column (Supplementary Fig. S1d and S8d). This suggests that the processes of formation of CHO compounds and those containing heteroatoms goes in parallel. The epipelagic is the layer with the highest formation of CHO compounds detected in the negative ionization mode (Fig. 6a).

4.4. Suggested mechanisms of early lipid transformation processes

A first proposed mechanism of CHO compound formation, regardless of the oceanic zone, is crosslinking or condensation at sites of unsaturation. It appears that this mechanism acts on lipids in general. Crosslinking is a proposed mechanism for the formation of highly unsaturated lipids that contain N (average DBE = 14) and P (average DBE = 6.7) in the molecular formula, whose molecular mass increases with depth. It has been suggested that crosslinking of transformed lipids could lead to the formation of humic substances (Gašparović et al., 2017, 2018b). The unimodal carbon number distribution of CHO compounds, in contrast to the bimodal distribution of reported lipids (Figs. 3 and 6, Supplementary Figs. S2 and S9) suggests crosslinking of reported lipids of lower and higher carbon content (lipid residues and molecular residues of other biochemicals may also be considered). This leads to the formation of CHO compounds with on average larger carbon content (CHO_Ep, CHO_Me, CHO_Ba and CHO_Ab), and which are more unsaturated than their counterparts, i.e., lipids present in living plankton (e.g. ReportedLipid_Ep) (Fig. 4b and Fig. 7b). Probably because of their greater unsaturation, these CHO compounds are more susceptible to degradation by abiotic and/or biotic processes, such as by microorganisms' extracellular and membrane-bound hydrolytic enzymes. Consequently, they are only found in the ocean zone where they are produced.

Another lipid transformation processes that occur simultaneously are partial degradation or fragmentation (decrease in C atoms) and double bond reduction (lower DBE and DBE/C). The CHO compounds formed during this transformation step are more stable to further transformation and are transferred deeper into the water column; for the example CHO_Ep-Ab lipids. Few of CHO compounds, from either ionization mode, were aromatic structures, suggesting that formation of aromatic structures is not an important process during early lipid transformation in the oceanic water column.

Bio/hydrogenation occurs mainly on CHO compounds detected by positive ionization mode (Figs. 5, S6 and S7). This process likely results in the formation of transformation/degradation less susceptible saturated CHO compounds. This could explain the much lower removal of CHO compounds detected in the positive ionization mode compared to the negative ionization mode. The highest abundance of saturated compounds observed for CHO Ep-Ab, CHO_Me-Ab and CHO_Ba_Ab confirm that the organic matter saturation is an important property for the export of carbon to the deep ocean. The widespread distribution of hydrogenase genes found in different bacteria and archaea in both oxic and anoxic aquatic environments (Greening et al., 2016) suggests that hydrogenation may occur throughout the water column. The importance of saturation for carbon export in the ocean is already observed for the uncharacterized lipids containing sulfur, and biologically relevant elements as N and P (Gašparović et al., 2017, 2018a, 2018b). The abundance, contribution to the total lipids, molecular diversity, and average molecular mass of saturated CHONP lipids, detected in the negative ionization mode, increased with depth. The proposed mechanisms for their formation are crosslinking and biohydrogenation (Gašparović et al., 2017). Hydrogenation in parallel with deoxygenation and increase in molecular mass (crosslinking) are the proposed mechanisms for the formation of novel (database unmatched) lipids that contain phosphorus

(Gašparović et al., 2018b). Hydrogenation is also proposed for the formation of novel sulfur containing lipids (Gašparović et al., 2018a).

Two other transformational processes that lead to CHO compound production are lipid oxidation and dehydrogenation (c.f. the van Krevelen diagrams, Figs. 5 and 8). Details of the transformation processes involved are given in Table 1. The more oxidized (O/C > 0.4) CHO compounds, which are detected as positive ions, are characterized by lower unsaturation with respect to the reported lipids, i.e., lipids from which they are derived. Their lower unsaturation is plausible because singlet oxygen-mediated photooxidation or enzyme-catalyzed oxidation can occur at the double bonds (Rontani and Belt, 2020). A higher O/C ratio than reported lipids, indicative of oxidation, was observed in unreported lipids containing S (Gašparović et al., 2018a), N, and P detected in positive ionization (Gašparović et al., 2017). The increase in the average O/C ratio of CHO compounds detected in positive ionization mode with depth indicates that oxidation occurs throughout the water column (Supplementary Fig. S6b). Without detailed experiments, it is difficult to explain why some lipid compounds are more susceptible to oxidation.

The main products of dehydrogenation are more recalcitrant CHO compounds (H/C < 1.5) (D'Andrilli et al., 2015). The proposed processes associated with dehydrogenation are (i) increasing unsaturation (very high average DBE content; 9.2–21.3 for those detected as positive ions and 11.1–16.6 for those detected as negative ions, which are higher than the DBE of the reported lipids), (ii) crosslinking or condensation (higher C content compared to the reported lipids), and (iii) cyclization (low H/C ratios indicating cyclic structures with no, fewer or more double bonds). The mechanism of formation of the cyclic compounds is explained by internal cyclization and aromatization of non-phenylic precursors (e.g. diunsaturated fatty acids) (Hartgers et al., 1995). However, these CHO compounds could also be produced from reported lipids that have lower H/C that are also mainly cyclic in nature. In addition to being biologically produced, unsaturated compounds can be chemically produced by photochemical processes (Ciuraru et al., 2015). It appears that crosslinking and dehydrogenation, i.e., the formation of high molecular weight compounds with a high degree of unsaturation, generally works for lipids, as the same molecular changes were observed for unidentified lipid compounds containing N and P (Gašparović et al., 2017, 2018b).

The discussed formation of CHO compounds could be schematically represented as follows (Fig. 9):

We assume that the proposed mechanisms of CHO compounds' formation can be regarded as general processes of early lipid transformation in the oceans. However, which of these processes would prevail depends on the complex relationship between the physical, chemical, and biological processes that influence the quality and quantity of lipids produced. Seasonal variability also remains an important issue and should be interrogated.

4.5. Unsaturated cyclic and acyclic compounds have different susceptibilities to degradation

It is generally accepted that unsaturated lipids are more susceptible to degradation, whether biotic or abiotic (e.g. Sun and Wakeham, 1994). Our data suggest that the position of the double bond in the lipid molecule, acyclic and cyclic, determines whether a lipid is more or less susceptible to degradation. Double bonds in the cyclic structures of the more recalcitrant CHO compounds are protected or less reactive than double bonds in the aliphatic structures. A good examples are more recalcitrant CHO_Ep-Ab lipids, which are found in the whole water column and detected in both positive and negative ionization modes (c.f. Table 1). They are highly unsaturated with average DBE values of 14.6 and 13.4, respectively, and DBE/C 0.41 and 0.39, respectively. These recalcitrant CHO compounds are likely precursors for the formation of marine humic substances. Hedges et al. (1992) found that marine humic substances are highly branched structures with 18–20% unsaturated carbon, suggesting interlinked (possibly cyclic) aliphatic carbon sequences.

4.6. Considerations on the future efficiency of the carbon sink through lipids

Global warming will affect ocean biogeochemical cycles (York, 2018). Warming affects the oceanic carbon cycle through a number of indirect changes that include reduced CO_2 solubility, ocean acidification, deoxygenation, increased ocean stratification that

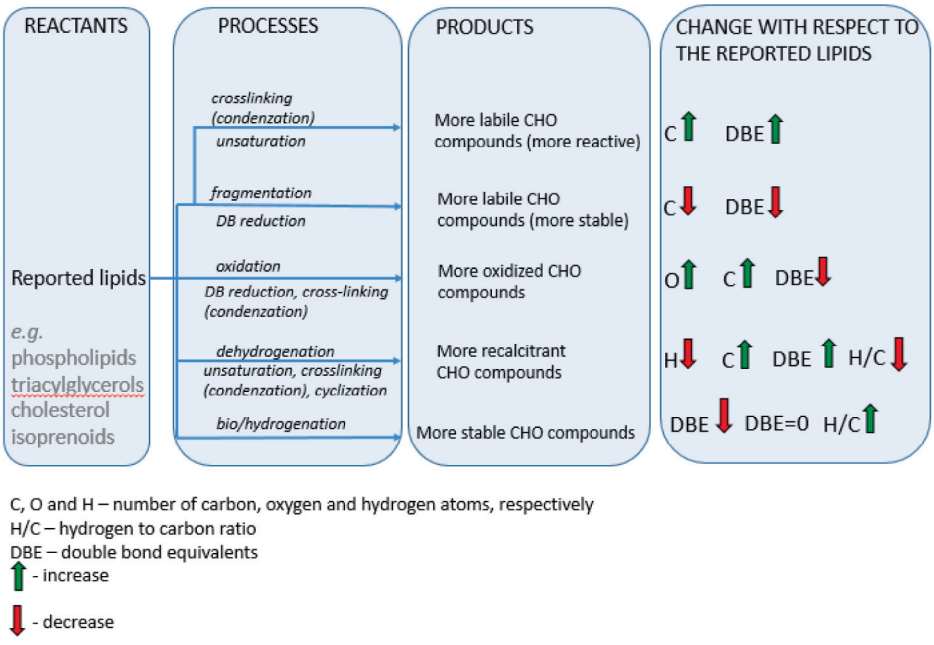

Fig. 9. A summary scheme highlighting the major findings of early lipid transformation processes.

reduces water column mixing (contributing to oligotrophication of the upper water column), and a reduction in thermohaline circulation. Hence, the efficiency of the carbon sink through lipids in the future ocean should be considered not only through the role of plankton in carbon sequestration, but also through the effects on processes acting on lipid transformation.

The metabolic content of lipids in phytoplankton (5–31% (Anderson, 1995)) is lower than that of proteins and sugars. However, recent research has shown that warming enhances lipid production by microalgae, especially those growing under oligotrophic conditions (e.g., Novak et al., 2019). The fatty acid composition of cell membranes depends, among other things, on temperature. As temperature increases, the proportion of saturated fatty acids increases (e.g., Fuschino et al., 2011). This suggests a negative feedback on global warming through the accumulation of lipids and especially saturated fatty acids, which are important for more efficient export of lipid carbon to the deep ocean. In addition, lipids are hydrophobic substances and therefore tend to adsorb onto sinking particles, contributing to carbon sequestration (Novak et al., 2018).

One of the consequences of global warming is the expected expansion of oxygen minimum zones (Lengger et al., 2019). Suboxic and hypoxic conditions already exist in large areas of the North Pacific, smaller areas of the South Pacific and North Indian Oceans, and the eastern tropical Atlantic and Pacific Oceans (Keeling et al., 2010). This would certainly reduce the oxidation efficiency of lipids, leading to the formation of less unsaturated lipids, and consequently will influence retarded drawdown of lipid carbon. Increased photooxidation would act in the opposite direction in the case of higher sunlight intensity due to lower cloud cover and vice versa. Higher temperatures will enhance the biotic transformation processes, peroxidation and biohydrogenation, mediated by enzymes, unless the temperature threshold for enzymes is exceeded. Since the rate of an enzyme-catalysed reaction increases with increasing temperature, it is expected that more refractory lipid transformation products (e.g., humic substances) will be produced, contributing to a positive feedback on ocean carbon sequestration. In summary, the efficiency of lipid carbon export to the deep ocean and sediment will depend on the success of mechanisms to form saturated and refractory compounds, including high molecular weight cyclic compounds with a high degree of unsaturation.

5. Conclusions

Here we describe CHO compounds formed as decomposition intermediates during early lipid transformation processes in the NE Atlantic Ocean. We show that early lipid transformation involves complex processes that include (i) crosslinking or condensation at the double bonds of known lipids or their residues; (ii) fragmentation (partial degradation) with concomitant reduction of the double bond, (iii) oxidation, leading to the formation of less unsaturated lipid transformation products; (iv) hydrogenation, leading to the formation of saturated or less unsaturated compounds; and (v) dehydrogenation followed by crosslinking, leading to higher unsaturation and molecular mass and cyclization. The data suggest that the double bonds in the cyclic structures are protected or less reactive than those in the aliphatic structures. The formation of aromatic structures is not a significant process during early lipid transformation in the oceanic water column.

We have found that CHO compounds detected as negative ions are more prone to degradation than those detected as positive ions. They are substantially depleted in the layers above the abyssal and their molecular diversity is lower. A large fraction of the CHO compounds observed as positive ions are efficiently transported into the abyssal, most likely enabled by low unsaturation and rapid transport by diatom and coccolithophorid remains.

Our work enlightens the early lipid degradation pathways in the four ocean zones of the NE Atlantic Ocean, and which is possibly representative of more general processes in the ocean. In the face of ocean warming, the efficiency of carbon sink through lipids in the future ocean should be considered not only through the role of plankton in carbon sequestration, but also through the effects on processes acting on lipid transformation.

Declaration of Competing Interest

The authors declare that they have no known competing financial interests or personal relationships that could have appeared to influence the work reported in this paper.

Acknowledgements

We thank the crew of the RRS James Cook. This work was funded by a grant from the Croatian Science Foundation under project IP-11-2013-8607, by the National Science Foundation (IIA-1301346). This work is a contribution to the European FP7 Projects EURO-BASIN and to the Natural Environment Research Council, UK, core programme. We thank the reviewers for their helpful comments.

Appendix A. Supplementary material

Supplementary material to this article can be found online at https://doi.org/10.1016/j.gca.2022.12.021.

References

Anderson, L.A., 1995. On the hydrogen and oxygen content of marine phytoplankton. Deep Sea Res. I 42, 1675–1680.
Arts, M.T., Ackman, R.G., Holub, B.J., 2001. "Essential fatty acids" in aquatic ecosystems, a crucial link between diet and human health and evolution. Can. J. Fish. Aquat. Sci. 58, 122–137.
Bartley, M., Boeing, W., Corcoran, A., Holguin, F., Schaub, T., 2013. Effect of salinity on growth and lipid accumulation of the biofuel microalgae *Nannochloropsis salina* and invading organisms. Biomass Bioenerg. 54, 83–88.
Bligh, E.G., Dyer, W.J., 1959. A rapid method of total lipid extraction and purification. Can. J. Biochem. Phys. 37, 911–917.
Brassell, S.C., 1993. Application of biomarkers for delineating marine paleoclimatic fluctuations during the Pleistocene. In: Engel, M.H., Macko, S.A. (Eds.), Organic Geochemistry. Plenum Press, New York, pp. 699–738.
Campos, H., Boeing, W., Dungan, B., Schaub, T., 2014. Cultivating the marine microalga *Nannochloropsis salina* under various nitrogen sources: Effect on biomass yields, lipid content and composition, and invasive species. Biomass Bioenerg. 66, 301–307.
Canuel, E.A., Martens, C.S., 1996. Reactivity of recently deposited organic matter: degradation of lipid compounds near the sediment-water interface. Geochim. Cosmochim. Acta 60, 1793–1806.
Ciuraru, R., Fine, L., van Pinxteren, M., D'Anna, B., Herrmann, H., George, G., 2015. Photosensitized production of functionalized and unsaturated organic compounds at the air–sea interface. Sci. Rep. 5, 12741.
Collins, J.R., Fredricks, H.F., Bowman, J.S., Ward, C.P., et al., 2018. The molecular products and biogeochemical significance of lipid photooxidation in West Antarctic surface waters. Geochim. Cosmochim. Acta 232, 244–264.
Derieux, S., Fillaux, J., Saliot, A., 1998. Lipid class and fatty acid distributions in particulate and dissolved fractions in the north Adriatic Sea. Org. Geochem. 29, 1609–1621.
D'Andrilli, J., Cooper, W.T., Foreman, C.M., Marshall, A.G., 2015. An ultrahigh–resolution mass spectrometry index to estimate natural organic matter lability. Rapid Commun. Mass Spectrom. 29, 2385–2401.
Fuschino, J.R., Guschina, I.A., Dobson, G., Yan, N.D., Harwood, J.L., Arts, M.T., 2011. Rising water temperatures alter lipid dynamics and reduce n–3 essential fatty acid concentrations in *Scenedesmus obliquus* (chlorophyta). J. Phycol. 47, 763–774.
Galois, R., Richard, P., Fricourt, B., 1996. Seasonal variations in suspended particulate matter in the Marennes-Oleron Bay, France, using lipids as biomarkers. Estuar. Coast. Shelf Sci. 43, 335–357.
Gašparović, B., Frka, S., Koch, B.P., Zhu, Z.Y., Bracher, A., et al., 2014. Factors influencing particulate lipid production in the East Atlantic Ocean. Deep-Sea Res. Pt. I 89, 56–67.

Gašparović, B., Penezić, A., Lampitt, R.S., Sudasinghe, N., Schaub, T., 2016. Free fatty acids, tri–, di– and monoacylglycerol production and depth–related cycling in the Northeast Atlantic. Mar. Chem. 186, 101–109.
Gašparović, B., Penezić, A., Lampitt, R.S., Sudasinghe, N., Schaub, T., 2017. Depth–related cycling of suspended nitrogen–containing lipids in the northeast Atlantic. Org. Geochem. 113, 55–66.
Gašparović, B., Penezić, A., Frka, S., Kazazić, S., Lampitt, R.S., et al., 2018a. Particulate sulfur–containing lipids: production and cycling from the epipelagic to the abyssopelagic zones. Deep-Sea Res. Pt. I 134, 12–22.
Gašparović, B., Penezić, A., Lampitt, R.S., Sudasinghe, N., Schaub, T., 2018b. Phospholipids as a component of the oceanic phosphorus cycle. Mar. Chem. 250, 70–80.
Goutx, M., Guigue, C., Striby, L., 2003. Triacylglycerol biodegradation experiment in marine environmental conditions, definition of a new lipolysis index. Org. Geochem. 34, 1465–1473.
Goutx, M., Wakeham, S.G., Lee, C., Duflos, M., Guigue, C., et al., 2007. Composition and degradation of marine particles with different settling velocities in the northwestern Mediterranean Sea. Limnol. Oceanogr. 52, 1645–1664.
Greening, C., Boswas, A., Carere, C.R., Jackson, C.R., Taylor, M.C., et al., 2016. Genomic and metagenomics surveys of hydrogenase distribution indicate H2 is a widely utilized energy source for microbial growth and survival. ISME J 10, 761–777.
Gérin, C., Goutx, M., 1994. Iatroscan–measured particulate and dissolved lipids in the Almeria-Oran frontal system (Almofront–1, May 1991). J. Mar. Sys. 5, 343–360.
Hartgers, W.A., Damste, J.S.S., de Leeuw, J.W., 1995. Curie–point pyrolysis of sodium–salts of functionalized fatty–acids. J. Anal. Appl. Pyrolysis 34, 191–217.
Hartman, S.E., Lampitt, R.S., Larkin, K.E., Pagnani, M., Campbell, J., et al., 2012. The Porcupine Abyssal Plain fixed–point sustained observatory (PAP–SO): variations and trends from the Northeast Atlantic fixed–point time–series. ICES J. Mar. Sci. 69, 776–783.
Hartman, S.E., Bett, B.J., Durden, J.M., Henson, S.A., Iversen, M., et al., 2020. Enduring science: three decades of observing the Northeast Atlantic from the Porcupine Abyssal Plain Sustained Observatory (PAP–SO). Prog. Oceanogr. 191, 102508.
Hedges, I.J., Hatcher, P.G., Ertel, J.R., Meyers-Schulte, K.J., 1992. A comparison of dissolved humic substances from seawater with Amazon River counterparts by 13CNMR spectrometry. Geochim. Cosmochim. Acta 56, 1753–1757.
Hedges, J.I., Baldock, J.A., Géinas, Y., Lee, C., Peterson, M., Wakeham, S.G., 2001. Evidence for non–selective preservation of organic matter in sinking marine particles. Nature 409, 801–804.
Holguin, F., Schaub, T., 2013. Characterization of microalgal lipid feedstocks by direct infusion FT–ICR mass spectrometry. Algal Res. 2, 43–50.
Hunter, J.E., Fredricks, H.F., Behrendt, L., Alcolombri, U., Bent, S.M., et al., 2021. Using high-sensitivity lipidomics to assess microscale heterogeneity in oceanic sinking particles and single phytoplankton cells. Environ. Sci. Technol. 55, 15456–15465.
Iversen, M.H., Lampitt, R.S., 2020. Size does not matter after all: No evidence for a size–sinking relationship for marine snow. Prog. Oceanogr. 189, 102445.
Juergens, M., Deshpande, R., Lucker, B., Park, J., Wang, H., et al., 2015. The regulation of photosynthetic structure and function during nitrogen deprivation in *Chlamydomonas reinhardtii*. Plant Physiol. 167, 558–573.
Keeling, R.F., Körtzinger, A., Gruber, N., 2010. Ocean deoxygenation in a warming world Ann. Rev. Mar. Sci. 2, 199–229.
Kendrick, E., 1963. A mass scale based on CH2=14.0000 for high resolution mass spectrometry of organic compounds. Anal. Chem. 35, 2146–2154.
Killops, S.D., Frewin, N.L., 1994. Triterpenoid diagenesis and cuticular peservation. Org. Geochem. 21, 1193–1209.
Killops, S., Killops, V., 2013. Introduction to Organic Geochemistry. Blackwell Publishing, Oxford.
Koch, B.P., Dittmar, T., 2006. From mass to structure: an aromaticity index for high–resolution mass data of natural organic matter. Rapid Comm. Mass Spectrom. 20, 926–932.
Kujawinski, E.B., Vecchio, R.D., Blough, N.V., Klein, G.C., Marshall, A.G., 2004. Probing molecular-level transformations of dissolved organic matter: insights on photochemical degradation and protozoan modification of DOM from electrospray ionization Fourier transform ion cyclotron resonance mass spectrometry. Mar. Chem. 92, 23–37.
Lampitt, R.S., Billett, D.S.M., Martin, A.P., 2010. The sustained observatory over the Porcupine Abyssal Plain (PAP): Insights from time series observations and process studies (preface). Deep-Sea Res. Pt. II 57, 1267–1271.
Lee, C., Wakeham, S., Arnosti, C., 2004. Particulate organic matter in the sea: the composition conundrum. Ambio 33, 565–575.
Lengger, S.K., Rush, D., Mayser, J.P., Blewett, J., Schwartz-Narbonne, R., et al., 2019. Dark carbon fixation in the Arabian Sea oxygen minimum zone contributes to sedimentary organic carbon (SOM). Glob. Biogeochem. Cycles 33, 1715–1732.
Lipp, J.S., Hinrichs, K.U., 2009. Structural diversity and fate of intact polar lipids in marine sediments. Geochim. Cosmochim. Acta 73, 6816–6833.
Loh, A.N., Canuel, E.A., Bauer, J.E., 2008. Potential source and diagenetic signatures of oceanic dissolved and particulate organic matter as distinguished by lipid biomarker distributions. Mar. Chem. 112, 189–202.
Macovei, V.A., Hartman, S.E., Schusterc, U., Torres-Valdésd, S., Moore, C.M., Sanders, R.J., 2020. Impact of physical and biological processes on temporal variations of the ocean carbon sink in the mid–latitude North Atlantic (2002–2016). Prog. Oceanogr. 180, 102223.
Martin, P., Lampitt, R.S., Perry, M.J., Sanders, R., Lee, C., D'Asaro, E., 2011. Export and mesopelagic particle flux during a North Atlantic spring diatom bloom. Deep-Sea Res. Pt. I 58, 338–349.
McDonough, L.K., O'Carroll, D.M., Meredith, K., et al., 2020. Changes in groundwater dissolved organic matter character in a coastal sand aquifer due to rainfall recharge. Water Res. 169, 115201.
McGrath, T., Nolan, G., McGovern, E., 2012. Chemical characteristics of water masses in the Rockall Trough. Deep-Sea Res. I 61, 57–73.
McKenna, A.M., Williams, J.T., Putman, J.C., et al., 2014. Unprecedented ultrahigh resolution FT–ICR mass spectrometry and parts–per–billion mass accuracy enable direct characterization of nickel and vanadyl porphyrins in petroleum from natural seeps. Energ. Fuel 28, 2454–2464.
Novak, T., Godrijan, G., Marić Pfannkuchen, D., Djakovac, T., Mlakar, M., et al., 2018. Enhanced dissolved lipid production as a response to the sea surface warming. J. Mar. Sys. 180, 289–298.
Novak, T., Godrijan, J., Marić Pfannkuchen, D., Djakovac, T., Medić, N., et al., 2019. Global warming and oligotrophication lead to increased lipid production in marine phytoplankton. Sci. Total Environ. 668, 171–183.
O'Brien, C.J., Peloquin, J.A., Vogt, M., Heinle, M., Gruber, N., et al., 2013. Global marine plankton functional type biomass distributions: coccolithophores. Earth Syst. Sci. Data 5, 259–276.
Parrish, C.C., Wangersky, P.J., Delmas, R.P., Ackman, R.G., 1988. Iatroscan–measured profiles of dissolved and particulate marine lipid classes over the Scotian slope and in Bedford Basin. Mar. Chem. 23, 1–15.
Rogers, R.P., Schaub, T.M., Marshall, A.G., 2005. Petroleomics: Mass spectrometry returns to its roots. Anal. Chem. 77, 20A–27A.
Rontani, J.-F., Belt, S.T., 2020. Photo– and autoxidation of unsaturated algal lipids in the marine environment: An overview of processes, their potential tracers, and limitations. Org. Geochem. 139, 103941.
Rontani, J.-F., Koblízek, M., 2008. Regiospecific enzymatic oxygenation of cis–vaccenic acid in the marine phototrophic bacterium Erythrobacter sp strain mg3. Lipids 43, 1065–1074.
Rontani, J.-F., Zabeti, N., Wakeham, S.G., 2009. The fate of marine lipids: Biotic vs. abiotic degradation of particulate sterols and alkenones in the Northwestern Mediterranean Sea. Mar. Chem. 113, 9–18.
Rumyantseva, A., Henson, S., Martin, A., Thompson, A.F., Damerell, G.M., et al., 2019. Phytoplankton spring bloom initiation: The impact of atmospheric forcing and light in the temperate North Atlantic Ocean. Prog. Oceanogr. 178, 102202.
Sheridan, C.C., Lee, C., Wakeham, S.G., Bishop, J.K.B., 2002. Suspended particle organic composition and cycling the equatorial Pacific Ocean. Deep. Sea Res. I 49, 1983–2008.
Stuermer, D.H., Harvey, G.R., 1978. Structural studies on marine humus – new reduction sequence for carbon skeleton determination. Mar. Chem. 6, 55–70.
Sun, M.Y., Wakeham, S.G., 1994. Molecular evidence for degradation and preservation of organic–matter in the anoxic black–sea basin. Geochim. Cosmochim. Acta 58, 3395–3406.
Sáenz, J.P., Grosser, D., Bradley, A.S., Lagny, T.J., Lavrynenko, O., et al., 2015. Hopanoids as functional analogues of cholesterol in bacterial membranes. Proc. Natl. Acad. Sci. U. S. A. 112, 11971–11976.
Taguchi, S., Laws, E.A., 1988. On the microparticles which pass through glass fiber filter type GF/F in coastal and open waters. J. Plankton Res. 10, 999–1008.
van Aken, H.M., 2000a. The hydrography of the mid–latitude northeast Atlantic Ocean I: The deep water masses. Deep-Sea Res. Pt. I 47, 757–788.
van Aken, H.M., 2000b. The hydrography of the mid-latitude Northeast Atlantic Ocean II: The intermediate water masses. Deep-Sea Res. I 47, 789–824.
Versteegh, G.J.M., Blokker, P., Wood, G., Collinson, M.E., Sinninghe Damsté, J.S., de Leeuw, J.W., 2004. An example of oxidative polymerization of unsaturated fatty acids as a preservation pathway for dinoflagellate organic matter. Org. Geochem. 35, 1129–1139.
Wakeham, S.G., Canuel, E.A., 2006. Degradation and preservation of organic matter in marine sediments. In: Volkman, J.K. (Ed.), The handbook of environmental chemistry, series: Reaction and processes: Marine organic matter: Biomarkers, isotopes and DNA, Vol. 2. Springer, Berlin, pp. 295–321.
Wakeham, S.G., Lee, C., 1993. Production, transport, and alteration of particulate organic matter in the marine water column. In: Engel, M.H., Macko, S.A. (Eds.), Organic Geochemistry. Plenum Press, New York, pp. 145–169.
Wakeham, S.G., Hedges, J.I., Lee, C., Peterson, M.L., Hernest, P.J., 1997a. Compositions and transport of lipid biomarkers through the water column and surficial sediments of the equatorial Pacific Ocean. Deep-Sea Res. Pt. II 44, 2131–2162.
Wakeham, S.G., Lee, C., Hedges, J.I., et al., 1997b. Molecular indicators of diagenetic status in marine organic matter. Geochim. Cosmochim. Acta 61, 5363–5369.
Wakeham, S.G., Peterson, M.L., Hedges, J.I., Lee, C., 2002. Lipid biomarker fluxes in the Arabian Sea, with a comparison to the equatorial Pacific Ocean. Deep-Sea Res. Pt. II 49, 2265–2301.
Xie, S.T., Lipp, J.S., Wegener, G., Ferdelman, T.G., Hinrichs, K.U., 2013. Turnover of microbial lipids in the deep biosphere and growth of benthic archaeal populations. Proc. Natl. Acad. Sci. U.S.A. 110, 6010–6014.
York, A., 2018. Marine biogeochemical cycles in a changing world. Nat. Rev. Microbiol. 16, 259.
Zonneveld, K.A.F., Versteegh, G.J.M., Kasten, S., Eglinton, T.I., Emeis, K.C., et al., 2010. Selective preservation of organic matter in marine environments; processes and impact on the sedimentary record. Biogeosciences 7, 483–511.